Site Effects Assessment Using Ambient Excitations

SESAME

European Commission – Research General Directorate
Project No. EVG1-CT-2000-00026 SESAME

Report of the

WP04

H/V Technique : Empirical Evaluation

Deliverable D16.04
Comparisons of experimentally and theoretically estimated transfer functions with the (H/V) spectral ratio and evaluation of the applicability of the latter in cases of linear or/and non-linear soil behaviour

June 2004

List of Contents

Summary p.2
Acknowledgements p.2
Chapter 1: Introduction p.3
Chapter 2: Experimental (H/V) spectral ratio in comparison with standard spectral ratio and receiver function of weak and strong motion data p.5
Chapter 3: Experimental (H/V) spectral ratio in comparison with theoretical estimations

Chapter 4: (H/V) spectral ratio and nonlinear site response

Appendix 1
Appendix 2
Appendix 3

List of Contributors (in alphabetical order)

Bard Pierre-Yves	LGIT, Grenoble, France
Cornou Cecile	LGIT, Grenoble, France
Dimitriou Petros	ITSAK, Thessaloniki, Greece
Faeh Donat	ETHZ, Zurich, Swiss
Hagshenas Ebrahim	LGIT, Grenoble, France
Hatzidimitriou Panagiotis	ITSAK/AUTH-Geolab, Thessaloniki, Greece
Panou Areti	ITSAK, Thessaloniki, Greece
Papazachos Costas	ITSAK/AUTH-Geolab, Thessaloniki, Greece
Savvaidis Alexandros	ITSAK, Thessaloniki, Greece
Tento Alberto	CNR, Milano, Italy
Theodulidis Nikos	ITSAK, Thessaloniki, Greece

Project coordinator:	Pierre-Yves Bard	LGIT, Grenoble, France
Task A Leader:	Kuvvet Atakan	UiB, Bergen, Norway
WP04 Leader:	Nikos Theodulidis	ITSAK, Thessaloniki, Greece

Summary

In this Report comparisons of experimentally and theoretically estimated transfer functions with the (H/V) spectral ratio and evaluation of the applicability of the latter in cases of linear or/and non-linear soil behaviour is attempted, under the framework of the **SESAME Project** (Site Effects Assessment Using Ambient Excitations, EC-RGD, Project No. EVG1-CT-2000-00026 SESAME), Task A (H/V technique), Work Package 04 (WP04– H/V Technique: Empirical Evaluation), is presented.

Acknowledgements

This project (Project No. EVG1-CT-2000-00026 SESAME) is supported by the European Commission – Research General Directorate. We thank all the technical personnel from all the participating institutions, who have helped in data collection.

Chapter 1: Introduction

The aim of the WP04 is - parallel to the theoretical and numerical analyses - to achieve a purely empirical, experimental assessment of the meaning of the horizontal to vertical component spectral ratio (H/V ratio) based on ambient noise measurements, in order to answer the following questions:

- Does H/V ratio provide a reliable estimate of the fundamental frequency at a given site ?
- Does H/V ratio indicate the frequency band over which the ground motion is amplified ?
- Does H/V ratio provide a quantitative estimate of the corresponding amplification or a lower bound estimate ?
- How does H/V ratio compare with damage distribution in modern cities ?
- Can we learn anything about the limitations in noise H/V technique related to non-linear soil behavior ?

The basic work of thei WP consist in comparing the site effect estimates obtained with classical, well accepted methods (site to reference spectral ratio on earthquake recordings) with H/V noise and earthquake ratios obtained at the same sites. To accomplish this task all available data within the consortium decided to be compiled in order to analyse them in a common and homogeneous way. All the partners have agreed and provided their earthquake and noise recordings obtained for site effect estimation at many different sites throughout Europe and elsewhere to the task leader. In addition, some more noise recordings have been acquired at sites where site effects have been reliably estimated, in particular, at numerous strong motion sites where strong motion recordings are available. After the noise recordings compiled they processed with the technique developed and agreed upon in Work Package 3 of the SESAME project. Then the experimental site transfer functions obtained from earthquake recordings were compared with the H/V ratios obtained from noise recordings, in terms of fundamental frequency and amplitude level. Finally, statistics can be derived from these comparison and empirical conclusions can be drawn as to the meaning of H/V ratio concerning site conditions and site amplification.

In this Report *("**Comparisons of experimentally and theoretically estimated transfer functions with the (H/V) spectral ratio and evaluation of the applicability of the latter in cases of linear or/and non-linear soil behaviour"** Deliverable D16.04:*) all noise and earthquake recordings already compiled, after they had been converted to SESAME Ascii Format (SAF). This sub-task started at the 27th month and the final Report integrated at the 38th month of the project. There was a shift / delay of about 11 months in the final Deliverable submission *[see next diagram of Milestones and Expected Results]*. This delay is due to the following reasons:

(i) Additional data, outside of Europe, enriched the SESAME noise/earthquake recordings database and consequently caused a time shift in converting existing data set from various formats to SAF.

(ii) The JSESAME software development integrated with a certain delay.

(iii) For a number of sites – especially at the Greek strong motion network – noise measurements were repeated due to "bad" noise recordings initially acquired.

WP04 - H/V Technique: Empirical Evaluation

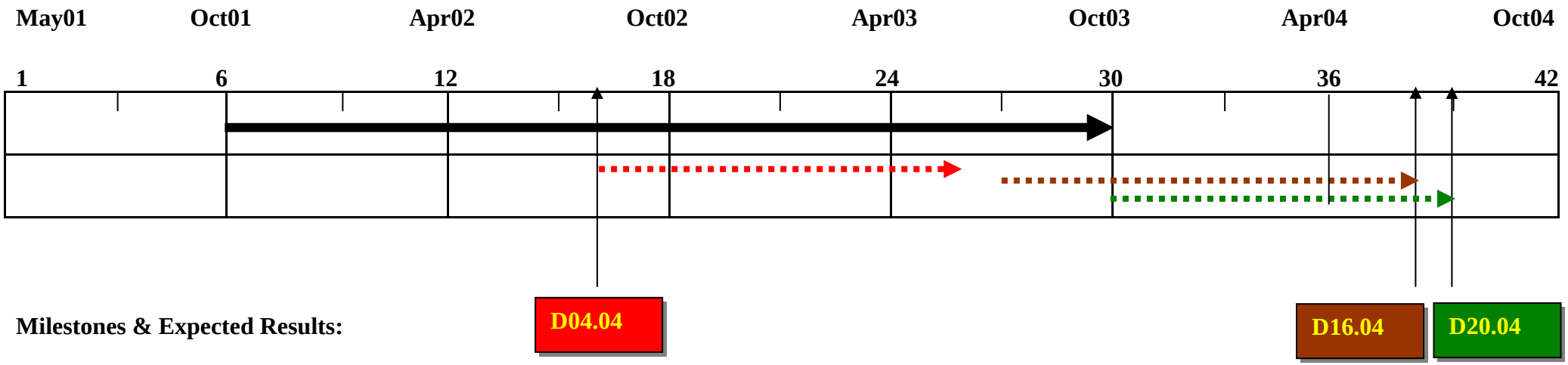

D04.04: Homogeneous Data Set of Noise and Earthquake Recordings at Many Sites

D16.04: Report Providing Comparisons of Experimentally and Theoretically Estimated Transfer Functions with the (H/V) Spectral Ratio Ambient Vibrations Technique and Evaluation of the Applicability of the Latter in Cases of Linear or/and non-Linear Soil Behavior

D20.04: Report Including Comparisons of Damage Distribution in Modern Urban Areas with Results from (H/V) Spectral Ratio

Chapter 2 : Experimental (H/V) spectral ratio in comparison with standard spectral ratio and receiver function of weak motion data

2.1. Processing results of the SESAME earthquake and ambient noise data set

In order to compare the results of ambient noise measurement with the more classic method spectral ratio, we processed the available earthquakes and ambient noise data of more than 18 sites European and also the Tehran (Iran).For all the earthquakes events, we have computed the spectra over a window including the whole signal (including P and S phases) and the site/reference spectral ratio has been calculated only at frequencies for which the signal to noise ratio (S/N) at both stations (reference and site under consideration) is greater than 3. Average spectral ratios and corresponding standard deviations were then derived from all available recording pairs. The same windows have been used to derive H/V spectral ratios from earthquake recordings. The H/V ratios for ambient noise were computed using some portions of the continuous recordings or preevent portion of earthquake data for the site that the specific noise measurement have not been done. For other sites analyzed noise windows were selected so as to avoid non-stationary transients. The Konno-Ohmachi (1998) smoothing method was used with b=40 and b=20 for all the projects.

We presented here (Figure 1, 8) the final results, on comparing the fundamental eigenfrequency and amplification amplitude obtained from ambient noise and earthquakes data. The frequencies and amplitudes presented here were extracted only for sites having more than five events with S/N ratio greater than 3 and the standard deviation less than 2.5 at that frequency.

We show the results one time only for the projects, for which the special noise measurements have been done so the noise H/V processing for them has been done by eliminating non-stationary transients (Figures 1, 3, 5, 7). In addition we show the result for all the projects ignoring the source of noise data (Figures 2, 4, 6, 8). As that can be seen there are a good agreement between fundamental frequency obtained from earthquake and ambient noise analyzing however there are the cases of non-agreements specially for low frequencies that noise data can not shown the fundamental frequency predicted spectral ratio method. Regarding the amplitude it can be seen that for many of the sites the amplification factors obtained from noise data are smaller than those obtained by earthquakes. The quantity plotted below H/V spectral ratios - except for the reference sites - is the number of the couples of events recorded at the site as well as at the reference station used for standard spectral ratio calculation. Plots for all examined sites are presented in ***Appendix 1.***

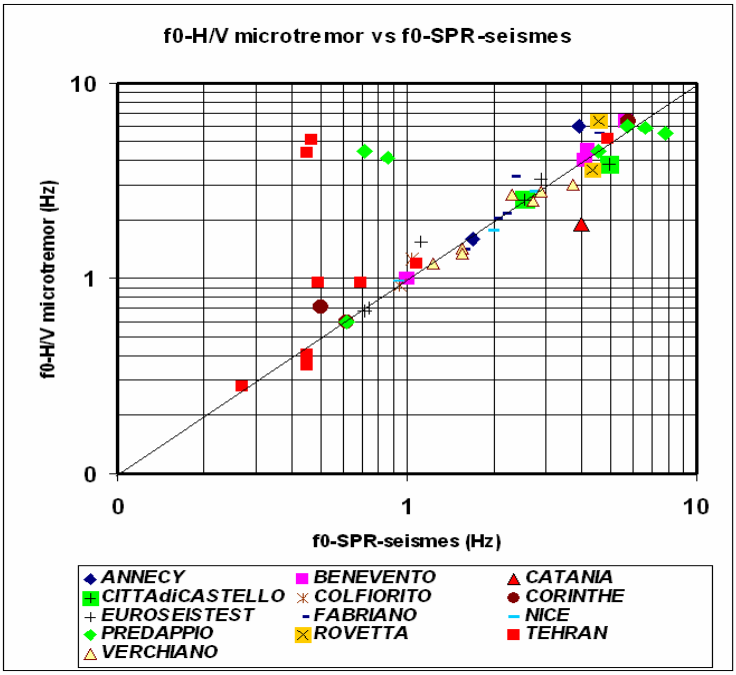

Figure 1. Fundamental eigenfrequency obtained from H/V method versus those obtained from classic spectral ratio method for project having specific microtremor measurements.

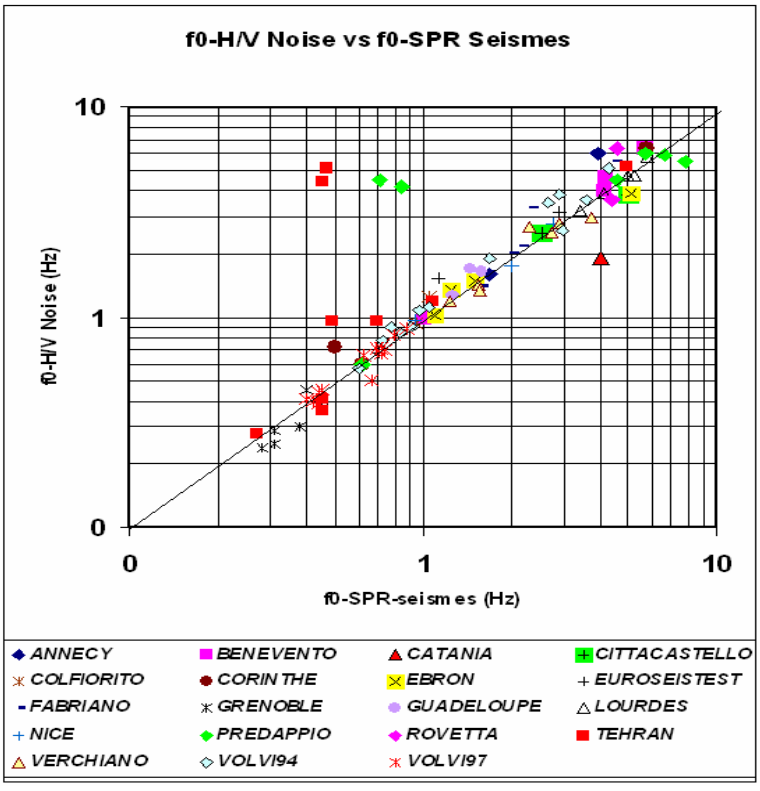

Figure 2. Fundamental eigenfrequency obtained from H/V method versus those obtained from classic spectral ratio method for all the projects.

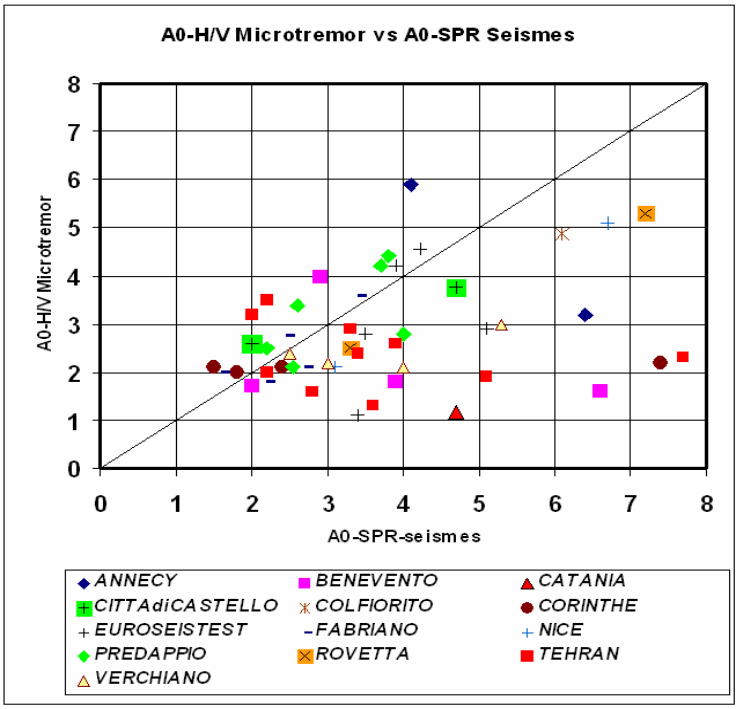

Figure 3. Amplification amplitude obtained from H/V method versus those obtained from classic spectral ratio method for project having specific microtremor measurements.

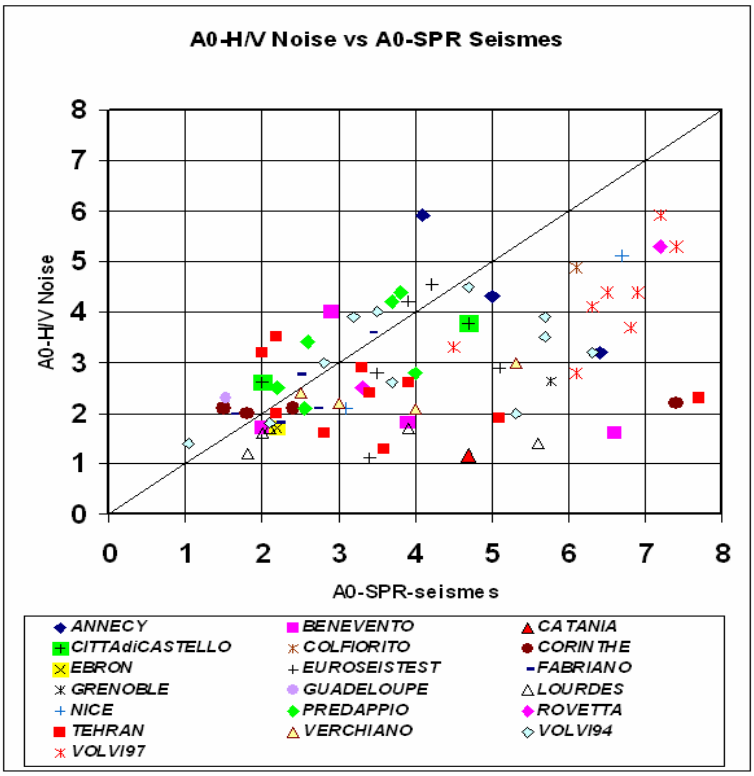

Figure 4. Amplification amplitude obtained from H/V method versus those obtained from classic spectral ratio method for all the projects.

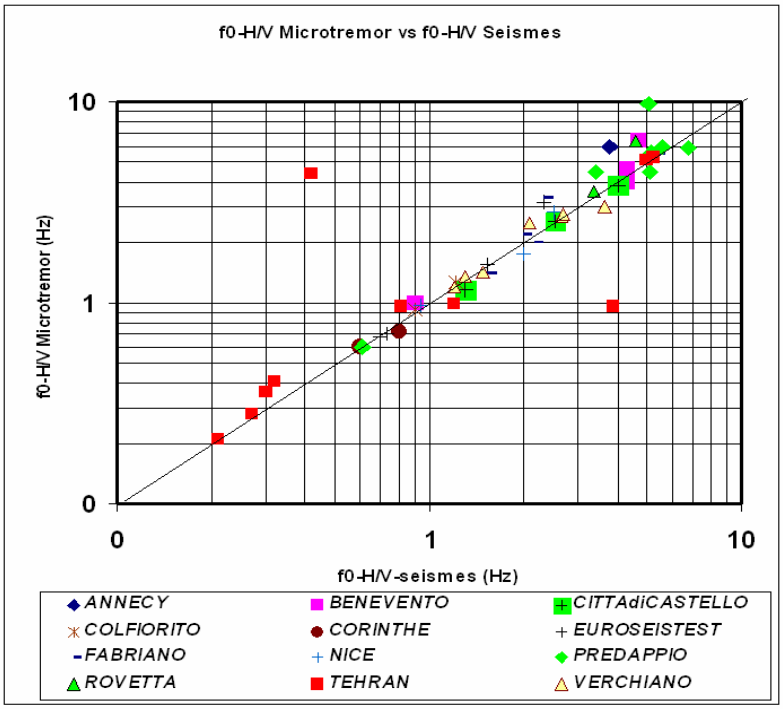

Figure 5. Fundamental eigenfrequency obtained from H/V method for noise versus H/V method for earthquakes for project having specific microtremor measurements.

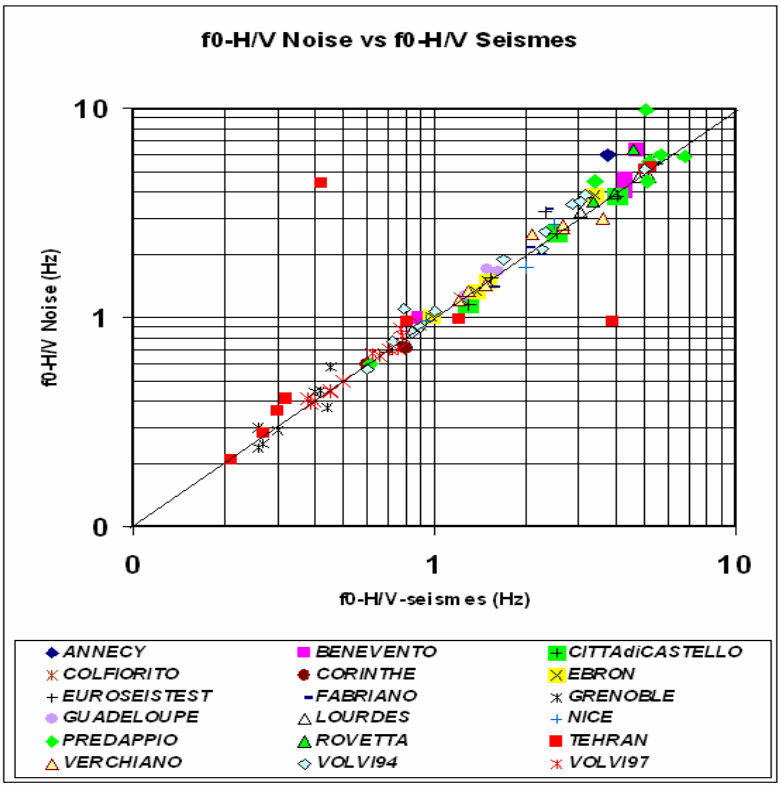

Figure 6. Fundamental eigenfrequency obtained from H/V method for noise versus H/V method for earthquakes for all the projects.

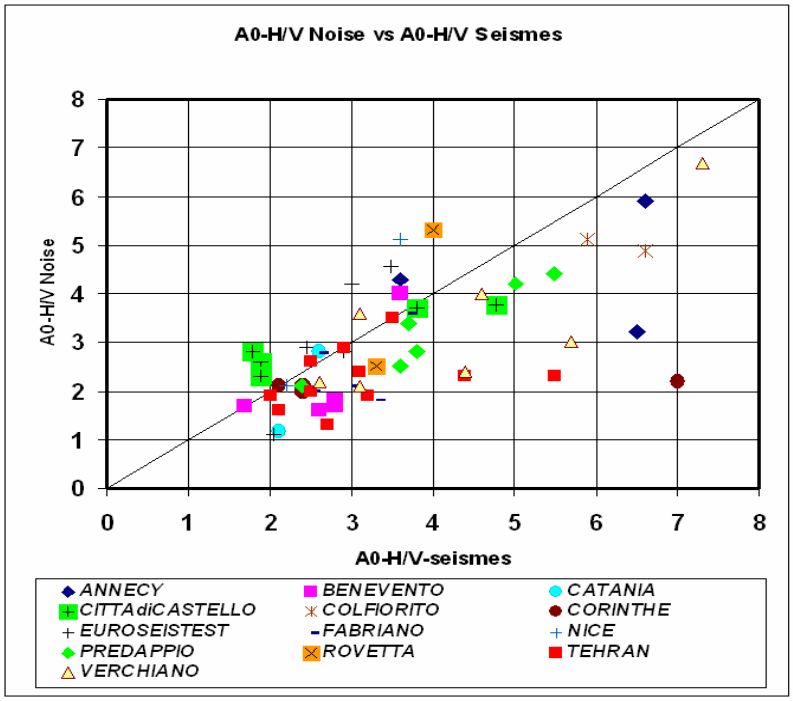

Figure 7. Amplification amplitude obtained from H/V method for noise versus H/V method for earthquakes for project having specific microtremor measurements.

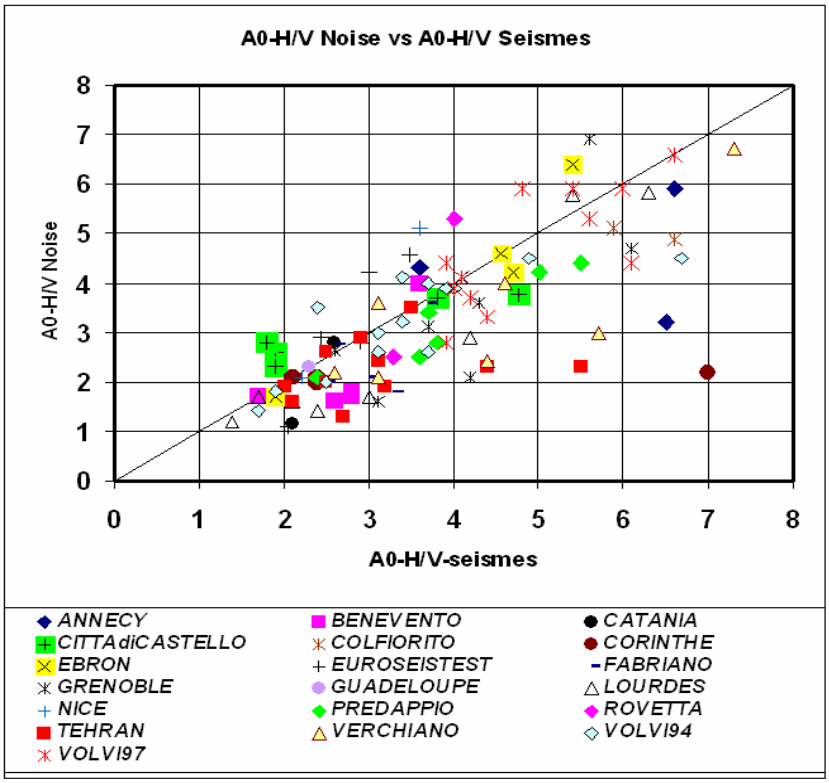

Figure 8. Amplification amplitude obtained from H/V method for noise versus H/V method for earthquakes for all the projects

2.2. Experimental (H/V) spectral ratio in comparison with receiver function of strong motion data

2.2.1. Ambient Noise Measurements at Strong Motion Network Sites

Data from strong motion network in Greece recorded at 62 sites were used to estimate receiver functions (H/V spectral ratio of earthquake recordings). Accelerograms for each station - using almost the entire record length - were classified according to strong motion duration, that is, in 10sec, 20sec, 30sec, 40sec and 60sec. In general, the longer the strong motion duration the largest the earthquake magnitude recorded. The majority of strong motion recordings come from analog type instruments (SMA-1). Strong motion data were uniformly processed taking into account the signal to noise ratio technique (Skarlatoudis et al. 2002, Theodulidis et al., 2004). Ambient noise measurements were performed only to the ITSAK network stations (Table 1) with 30 minutes duration each.

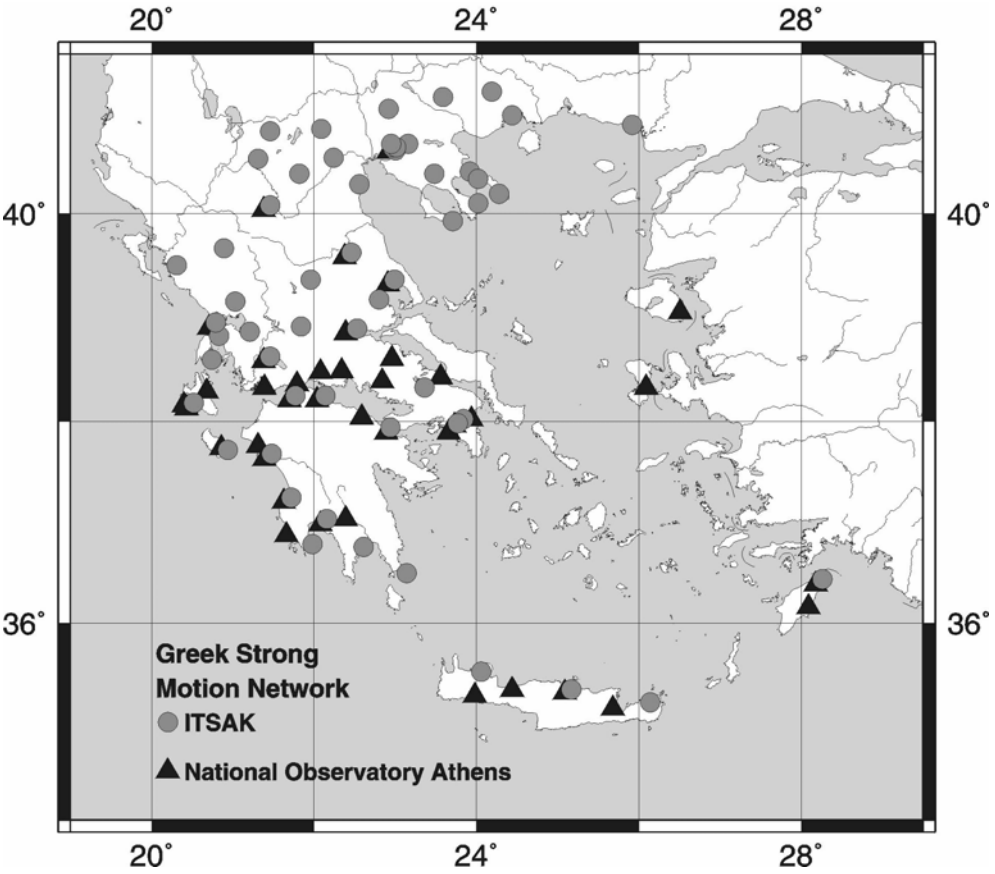

Figure 1. National strong motion network in Greece.

Table 1. Information on Greek strong motion network sites.

Site Code	Site Name	Latitude	Longitude	Orientation L-component	Site Characterization
ABS1	Ag. Basilios	40,650	23,100	S185W	B
AGR1	Agrinio	38,621	21,406	S261W	D
AIG1	Aigio	38,250	22,067	N70E	C
ALM1	Almiros	39,181	22,761	S189W	C
AML1	Amfilochia	38,858	21,160	N36E	B
ANS1	Ag. Nicolaos	36,472	23,101	W318N	B
ARG1	Argostoli	38,167	20,483	N59E	C
ART1	Arta	39,158	20,984	N55E	C
ATH2	Athens	38,018	23,789	N36E	C
ATH3	Athens	37,972	23,706	N46E	C
ATH4	Athens	37,996	23,743	N70E	C
CHN1	Chania	35,518	24,019	N39E	C
DRA1	Drama	41,139	24,142	N74E	C
EDE1	Edessa	40,805	22,051	N77E	C
FLO1	Florina	40,787	21,404	S257W	B
GRE1	Grevena	40,086	21,425	W330N	C
GTH1	Githio	36,754	22,567	N46E	A/B
HER1	Heraklio	35,318	25,102	E99S	C
IER1	Ierissos	40,391	23,873	N38E	C
IGM1	Igoumenitsa	39,503	20,268	N90E	A/B
JAN1	Jannina	39,659	20,851	W290N	C
KAL1	Kalamata	37,033	22,100	E180S	C
KAR1	Karditsa	39,366	21,920	E99S	C
KAS1	Kastoria	40,518	21,259	S260W	B
KAT1	Katerini	40,267	22,500	N41E	C
KAV1	Kavala	40,935	24,403	N87E	B
KIL1	Kilkis	40,990	22,869	S234W	C
KOR1	Korinthos	37,939	22,933	S216W	D
KOZ1	Kozani	40,302	21,784	W342N	B
KRN1	Koroni	36,802	21,961	W305N	B
KRP1	Karpenisi	38,917	21,800	N54E	A/B
KYP1	Kyparissia	37,250	21,667	N27E	B
LAM1	Lamia	38,902	22,425	W345N	B
LAR1	Larisa	39,637	22,417	S189W	C
LEF1	Lefkada	38,826	20,702	N65E	D
OUR1	Ouranoupolis	40,326	23,974	N48E	B
PAL1	Paliouri	39,935	23,673	E112S	C
PAT1	Patra	38,250	21,733	E150S	C
PAT2	Patra	38,238	21,738	E110S	C

PAT3	Patra	38,254	21,738	N12E	D
POL1	Poligiros	40,374	23,438	W328N	B
PRE1	Preveza	38,956	20,755	N90E	C
PYR1	Pyrgos	37,670	21,438	W351N	D
ROD1	Rodos	36,433	28,233	W288N	C
ROD2	Rodos	36,433	28,233	N54E	B
ROD3	Rodos	36,433	28,233	S185W	C
ROD4	Rodos	36,433	28,233	S250W	C
SAR1	Sarti	40,091	23,974	W330N	C
SER1	Serres	41,085	23,541	W296N	C
SIT1	Sitia	35,216	26,104	S207W	C
THE2	Thessaloniki	40,617	22,967	W352N	B
THE3	Thessaloniki	40,633	22,933	NS	D
THE4	Thessaloniki	40,517	23,017	N77E	D
THE5	Thessaloniki	40,633	22,933	W329N	D
THE6	Thessaloniki	40,633	22,933	E113S	D
THE7	Thessaloniki	40,633	22,933	NS	C
THV1	Thiva	38,317	23,317	S266W	C
TMN1	Thessaloniki	40,667	22,900	S257W	D
VAS1	Vasiliki	38,626	20,605	N20E	C
VER1	Veria	40,526	22,203	E158S	A/B
VOL1	Volos	39,366	22,951	E126S	C
ZAK1	Zakynthos	37,785	20,900	S230W	D

Data Processing

From 30 minutes each noise recording transient and spikes were visually removed in order to keep as much as the stationary part of the ambient noise recording. Then the remaining recording was divided in a certain number of windows of 20secduration each. For all examined sites the number of selected 20 sec windows was greater than 15. Using SEISAN code the FFT of all three components - vertical, NS, EW - calculated and the average H/V spectral ratio ± 1 standard deviation, were estimated. For smoothing Fourier amplitude spectra the moving average technique was performed. The same code was used to estimate the H/V spectral ratio (receiver function) of the strong motion recordings for each site examined. The unique difference between ambient noise and strong motion data was in the short 10 sec duration strong motion recordings, that is, half the defined window length for further processing. Two hundred nineteen comparisons between H/V ambient noise and H/V strong motion spectral ratio (receiver function) for sixty two strong motion sites are presented in ***Appendix 2***. For those sites where more than five strong motion recordings exist, average ± 1 standard deviation is given. For the same ambient noise data set the JSESAME v1.05 code was also used. Comparison of the H/V spectral ratios between SEISAN and JSESAME code results, for all sites examined, is given in ***Appendix 3***. No significant differences in terms of fundamental frequencies, fo, and corresponding amplitude, Ao, was observed.

In Figures 2 and 3, distribution of the fundamental frequency, fo, with corresponding amplification, Ao, for noise and strong motion recordings, respectively, are shown. Fundamental frequencies for ambient noise H/V spectral ratio vary between 0.3HZ to 20Hz and for strong motion recordings between 0.4Hz to 20Hz. Corresponding amplitudes, Ao, for both data sets vary between 1.5 to about 10.

In Figures 4 and 5, comparison of ambient noise and strong motion recordings fundamental frequencies, respectively, for both components (Fo,e : EW/Vertical, Fo,n: NS/Vertical), are shown. For the majority of the examined sites both components showed comparable values. However, there are a few exceptions probably implying 2D site effects.

In Figure 6, comparison of fundamental frequency, fo, between ambient noise [Fo-Noise] and strong motion recordings [Fo-SM] for both horizontal components (blue diamonds: NS/Vertical, red squares: EW/Vertical) is shown. Although scattering of the compared Fo values is observed, for frequencies up to 9 Hz there is a remarkable correlation. This is in agreement with a relevant comparison between Fo from noise and Fo from weak motion earthquake recordings (see Chapter 2.1). In Figure 7, comparison of peak amplification between ambient noise [Ao-noise] and strong motion recordings [Ao-smdata] for both horizontal components (blue diamonds: NS/Vertical, red squares: EW/Vertical) is shown. In fact, there is no correlation between Ao-noise and Ao-smdata, as it was also found for weak motion earthquake recordings (see Chapter 2.1).

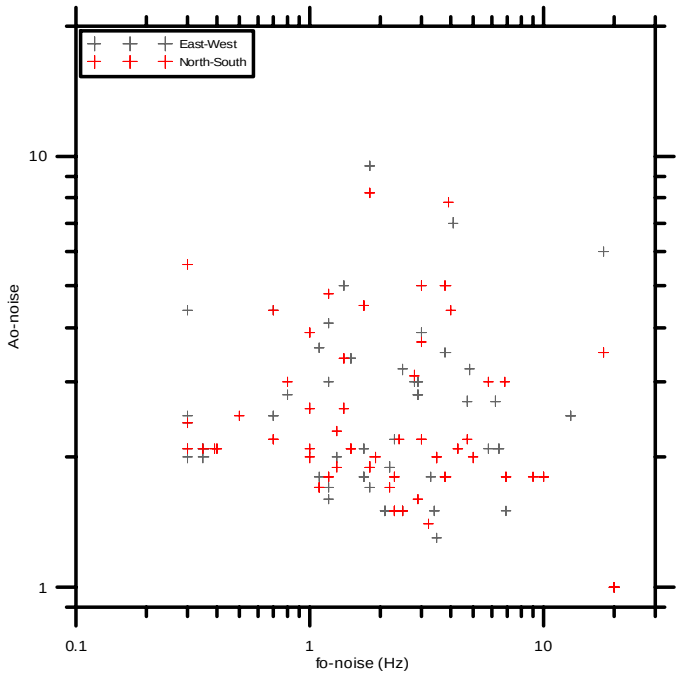

Figure 2. Distribution of the fundamental frequency, fo, with corresponding amplification, Ao, for noise recordings.

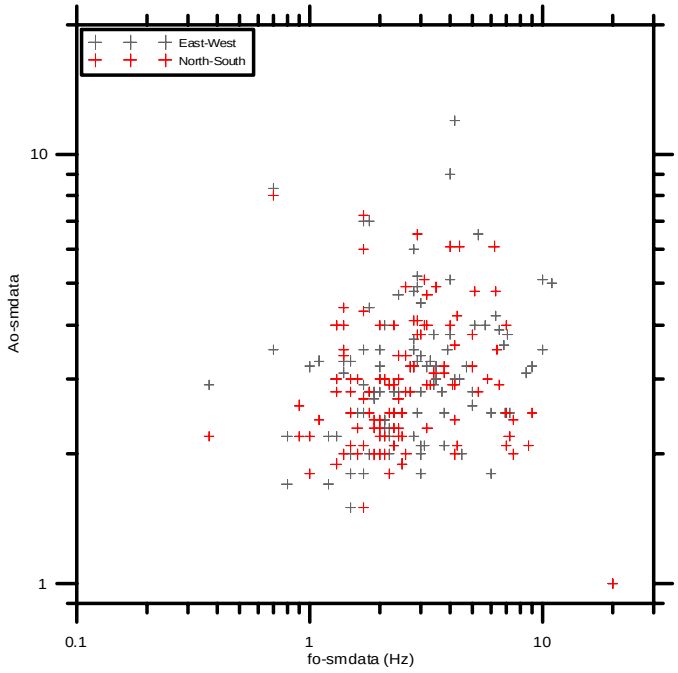

Figure 3. Distribution of the fundamental frequency, fo, with corresponding amplification, Ao, for strong motion recordings.

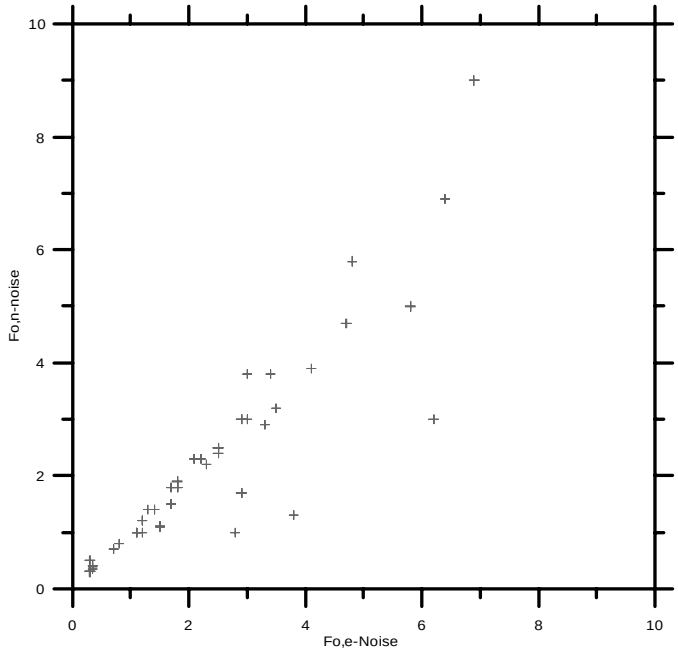

Figure 4. Comparison of ambient noise fundamental frequency for both components (Fo,e : EW/Vertical component, Fo,n: NS/Vertical component).

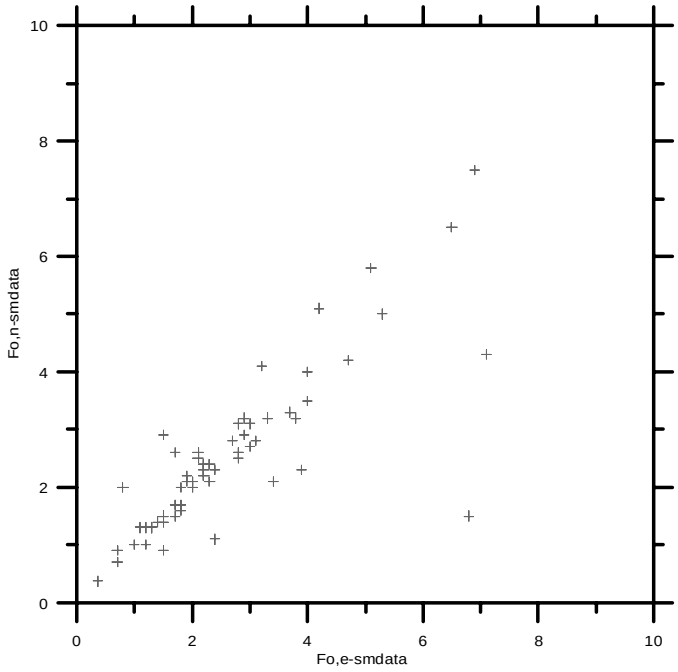

Figure 5. Comparison of strong motion recordings fundamental frequency for both components (Fo,e : EW/Vertical component, Fo,n: NS/Vertical component).

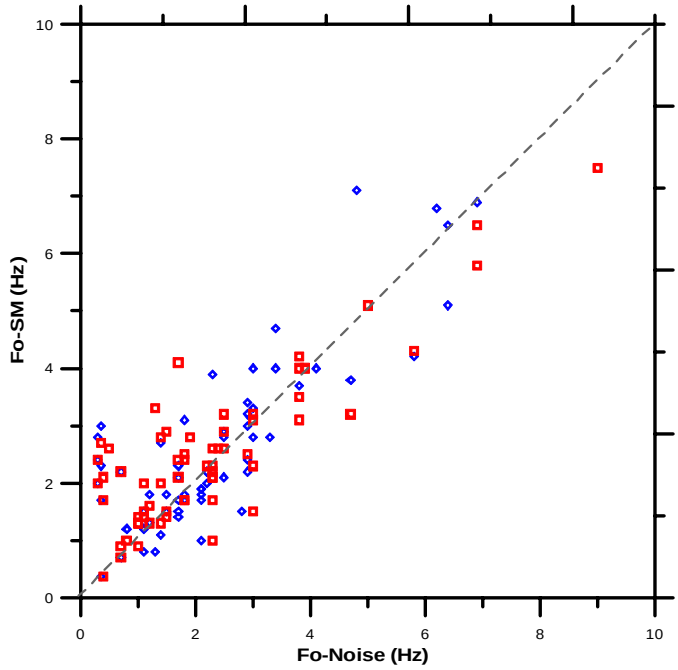

Figure 6. Comparison of fundamental frequency, fo, between ambient noise [Fo-Noise] and strong motion recordings [Fo-SM] for both horizontal components (blue diamonds: NS/Vertical, red squares: EW/Vertical).

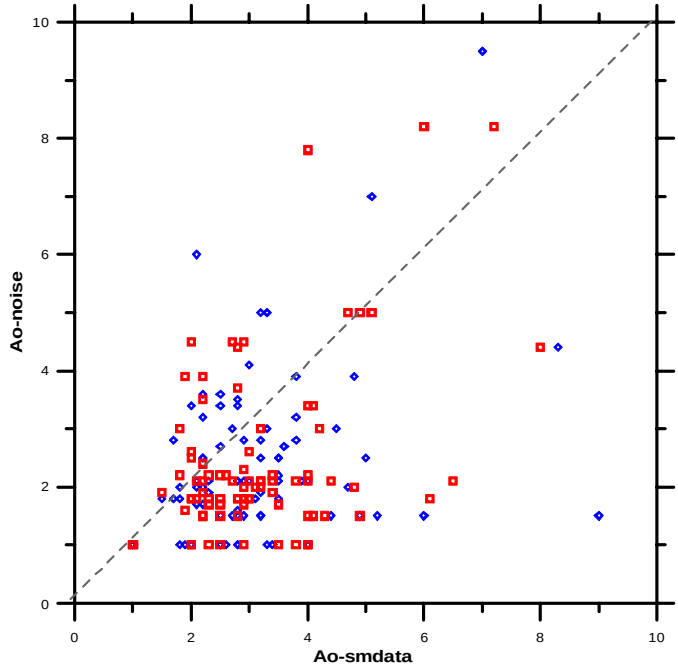

Figure 7. Comparison of peak amplification between ambient noise [Ao-noise] and strong motion recordings [Ao-smdata] for both horizontal components (blue diamonds: NS/Vertical, red squares: EW/Vertical).

Chapter 3: Experimental (H/V) spectral ratio in comparison with theoretical estimations

3.1. Inversion of local S-wave velocity structures from average H/V ratios, and the comparison with cross-hole measurements

3.1.1. Introduction

H/V spectral ratios from microtremors can be used to retrieve the S-velocity structure from a single ambient vibration record, by using its relation to the ellipticity of the fundamental mode Rayleigh wave and the amplitude of observed H/V ratio (Yamanaka et al., 1994, Satoh et al., 2001; Fäh et al., 2001). Constraints are needed in order to restrict the range of solutions, and the inversion is applied to sites where the thickness of the unconsolidated sediments is approximately known from borehole information. Within the uncertainty, the inverted structures generally agree well with the results from other S-wave measuring techniques such as down-hole and cross-hole measurements, and the analysis of ambient vibrations measured on an array (Fäh et al., 2003). Therefore this H/V technique can be used to check measurements from other S-wave measurement techniques or to constrain inversions for S-wave velocity profiles for example from ambient vibration array measurements.

We focus in this experiment on the comparison between the results from the H/V method to estimate S-wave velocities and cross-hole measurements for two sites in Greece. S-wave cross-hole measurements involves body waves in the frequency range above 30Hz, which on one hand allows to map sub-surface interface variations, but on the other hand operates in a frequency range above the frequency band of interest in engineering seismology. High-frequency waves may be strongly affected by small-scale lateral heterogeneities, and the measured velocities may not necessarily coincide with S-velocities in the frequency band below 10 Hz. The two examples shown here provide one comparison with good agreement and one with no satisfactory agreement between the results from the H/V method and the cross-hole measurements.

The method to obtain S-wave velocity structures from H/V spectral rations is described in Fäh et al. (2001, 2003). Two methods are first applied to compute average H/V ratios, a classical method based on the Fourier transform of the recordings and a method based on frequency-time-analysis (FTAN). In a second step, models are searched for which the ellipticity of the fundamental mode Rayleigh wave explains the observed H/V ratio. A third step involves numerical simulation of H/V spectral ratios for the inverted models, and a selection of the models that qualitatively explain the observed amplitude of the H/V peak. In this work the aforementioned methodology is applied for two sites in Greece, namely Nestos and Edessa, where cross-hole measurements are available. Results of these approaches are compared and discussed.

3.1.2. Site description and data

Our test sites are two locations in northern Greece, the site NESTOS and the site EDESSA (Fig 1), where S-wave profiles where obtained from cross-hole measurements every 2m up to 64m depth.

Figure 1. Map of Greece indicating the two test sites Nestos and Edessa where ambient noise and cross-hole measurements were acquired.

At site NESTOS three profiles (CH2, CH3, CH5) have been measured that are located within a distance of 380 m (ITSAK-Gazetas, 2003). At each site 30 minutes of ambient vibration measurements have been recorded using CityShark 24bits A/D recorder with Lenartz 3D/5sec sensor. Site geology is shown in Fig. 2 consisting of fluvial deposits containing clean sand and silty sand in a medium-dense to loose state overlaying weathered gneiss of unknown thickness (ITSAK-Gazetas, 2003; Klimis et al. 2004).

The local geology of the city of Edessa is quite complex. Ophiolithic formations, flysch and limestones and schists are found in the vicinity of the city. The most striking geological characteristic underlying the city is a thick layer of travertine (porous rock) with a maximum thickness of about 100m (Pitilakis et al. 1992). A thin layer of lacustrine and continental deposits with a thickness varying from a few to about 30m, is overlying the travertine. Borehole at the site under investigation showed 15.3m deposits overlain a 4m layer of weathered travertine (AUTH-ITSAK-YPEXODE, 1996).

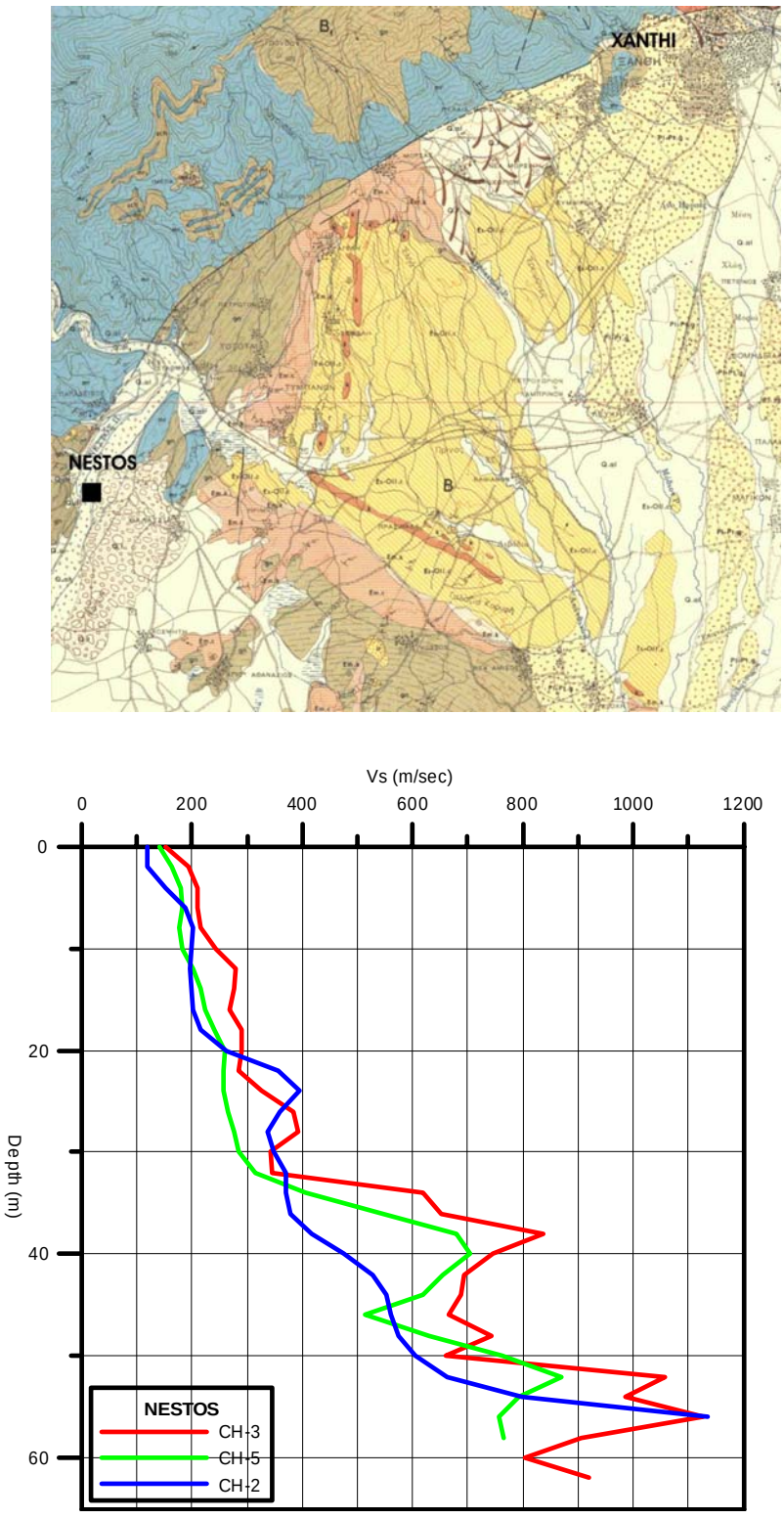

Figure 2. Regional surface geology in the vicinity of Nestos site [black square] (Q.al , Q.t : Fluvial deposits, Gn: Gneiss) and shear wave velocity profile from cross-hole measurements within a distance of 380m (ITSAK and Gazetas, 2003).

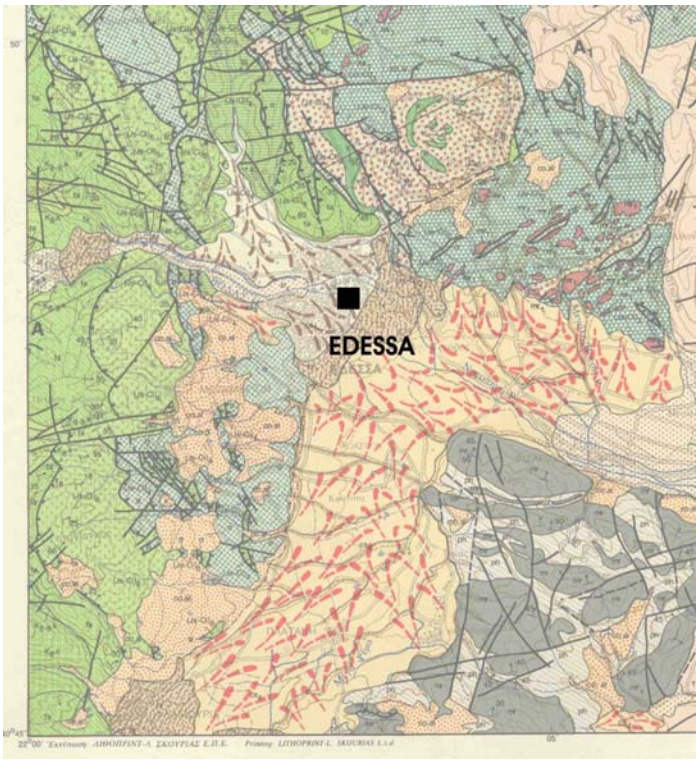

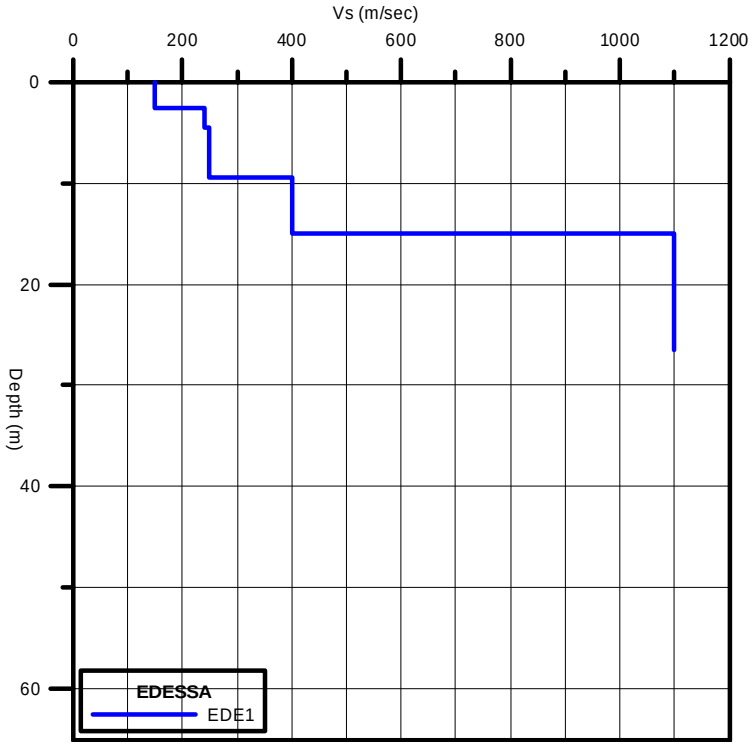

Figure 3. Regional surface geology in the vicinity of Edessa site [black square] (cs5: Recent Torrential Cones, Tv: Travertine, $(Js\text{-}Ci)_6$:Volcano-sedimentary series of Messimeri, $(Js\text{-}Ci)_5$: Volcanic Formation) and shear wave velocity profile from cross-hole measurements. (AUTH-ITSAK-YPEXODE, 1996).

3.1.3. Results for site NESTOS

For the site NESTOS CH2 several inverted structures obtained from the H/V method are shown in Figure 4a, with the corresponding ellipticity of the fundamental mode Rayleigh wave overlaid to the H/V ratios of the measurements in Figure 4b. The red curve in Figure 4a corresponds to the S-wave velocity obtained from cross-hole measurements. The inversion applied in the H/V method is resolving with good accuracy the soft-sediment structure, but does not allow an accurate estimate of the velocity of the bedrock. The scatter in the velocity models from the H/V method is increasing with depth. The ellipticities are all in good agreement with the observed H/V ratios, as does the ellipticity obtained for the model from cross-hole measurement (Fig 5). From the amplitude of the H/V ratio at the fundamental frequency of resonance (Fig.4b) it is concluded that the bedrock has rather low velocities below about 1400m/s, with a considerable thickness of more than 300 meters.

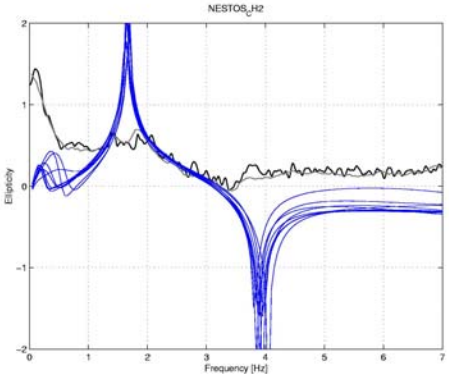

Figure 4 (a). Structural models obtained from the different inversions of the observed H/V ratios (blue lines) at site NESTOS CH2, compared to the model obtained from cross-hole measurements (ITSAK-Gazetas, 2003) (red line).

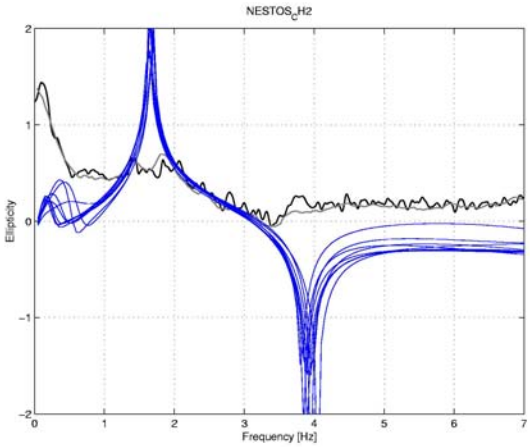

Figure 4(b). Comparison between H/V ratios of observed noise at site NESTOS CH2 (thin black line: classical method; thin gray line: FTAN based) and the ellipticity of the fundamental-mode Rayleigh waves for the inverted structures (blue curves).

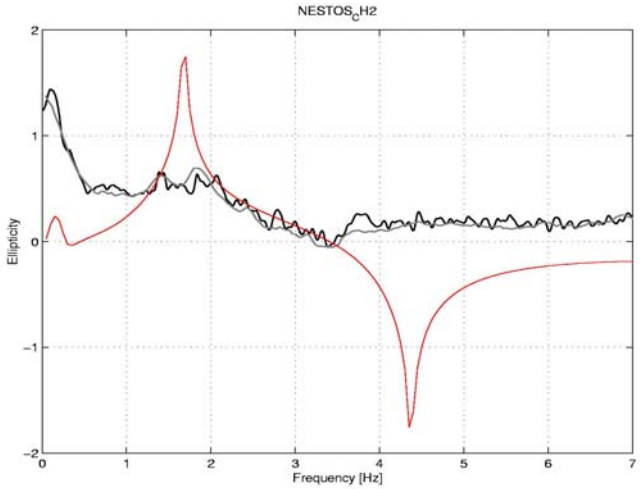

Figure 5. Comparison between H/V ratios of observed noise at site NESTOS CH2 (thin black line: classical method; thin gray line: FTAN based) and the ellipticity of the fundamental-mode Rayleigh wave for the model obtained from cross-hole measurements (red curve).

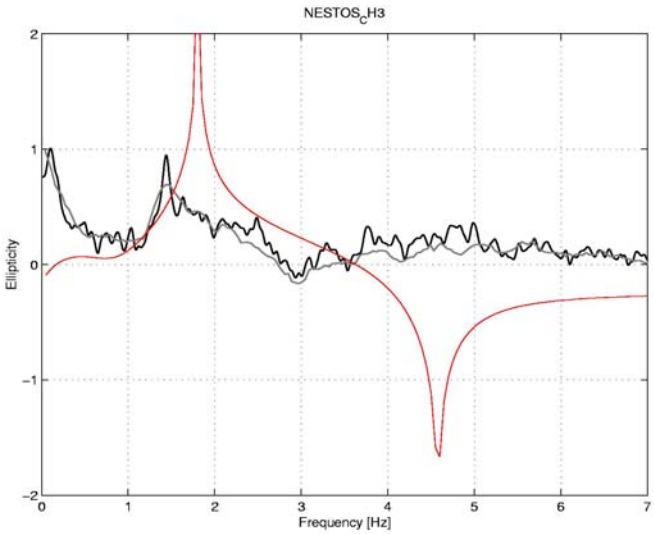

Figure 6 (a). The same as in Figure 5 but for site NESTOS CH3.

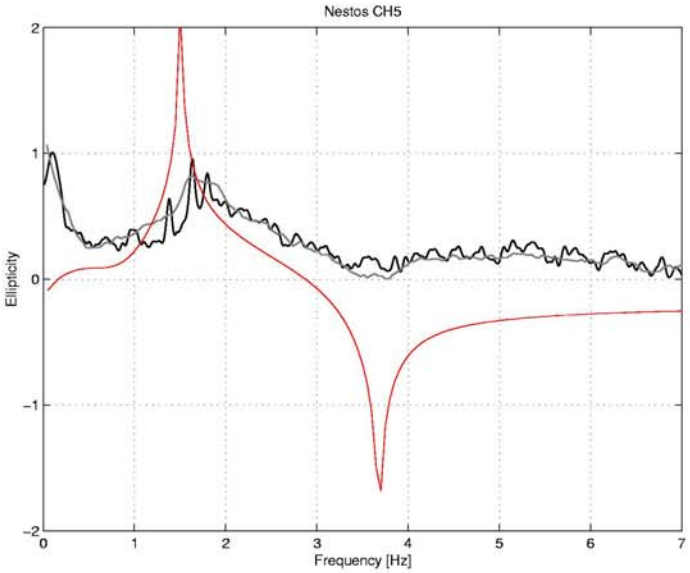

Figure 6 (b). The same as in Figure 5 but for site NESTOS CH5.

For sites NESTOS CH3 and CH5 (see Fig. 6), the comparison between ellipticity of the S-wave model from the cross-hole measurements and the measured H/V ratio is not as good as for site CH2. Reasons could be the high lateral variability of the soft sediments and the frequencies of the waves used in the cross-hole measurements. These differences are still within the accuracy of the cross-hole method. Another reason could be that the working hypothesis in the H/V method is not completely fulfilled, namely the dominance of the fundamental mode Rayleigh wave in the observed ambient vibration wavefield.

3.1.4. Results for site EDE1

For the site EDE1 several inverted structures obtained from the H/V method are shown in Figure 7a, with the corresponding ellipticity of the fundamental mode Rayleigh wave overlaid to the H/V ratios of the measurements in Figure 7b. For the inversion, the thickness of the soft sediments has been fixed, using the borehole information at this site. From the comparison between synthetic and observed amplitudes of H/V ratios at the fundamental frequency of resonance we distinguish between possible models (in green), good models (in blue) and a preferred model (in magenta). The red curve in Figure 7b corresponds to the result from the cross-hole measurement. The ellipticities from the models obtained with the H/V method are obviously all in good agreement with the observed H/V ratios. This is not the case for the model from cross-hole measurement (Fig 7b). This disagreement cannot be explained anymore with the variability of S-waves in the soft sediments. This site requires a revision of the local structural model. Either S-wave velocities are much lower as given in Figure7a, or the interface between soft sediments and bedrock is at larger depth. Travertine is a porous rock, and probably has a rather low S-wave velocity. The real rock interface may be at the volcanic-sedimentary floor, but this depth is not known. By defining this interface at larger depth, the inversion applied in the H/V method would result in higher S-wave velocitites.

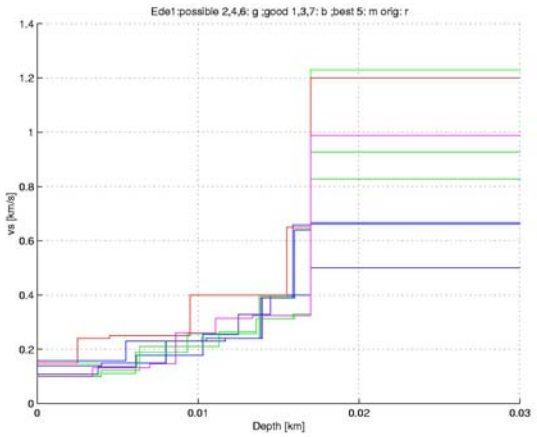

Figure7 (a). Structural models obtained from the different inversions of the observed H/V ratios (green lines: possible models; blue lines: good models; magenta line: preferred model) at site EDE1, compared to the model obtained from cross-hole measurements (AUTH-ITSAK-YPEXODE, 1996) (red line).

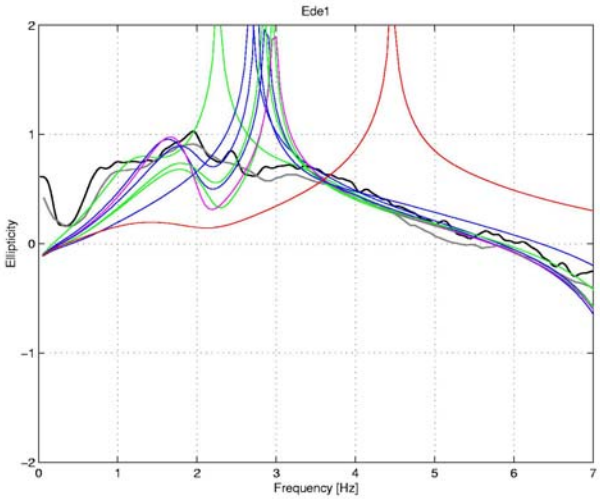

Figure 7 (b).
Comparison between H/V ratios of observed noise at site EDE1 (thin black line: classical method; thin gray line: FTAN based) and the ellipticity of the fundamental-mode Rayleigh waves for the inverted structures (green lines: possible models; blue lines: good models; magenta line: preferred model). The red curve is the ellipticity obtained for the model from the cross-hole measurements.

References

Aki, K., 1957, Space and time spectra of stationary stochastic waves with special reference to microtremors. Bull. Earthquake Res. Inst., Tokyo Univ. 35, 415-457.

AUTH-ITSAK-YPEXODE, 1996, Site Effects Study and Dynamic Soil-Structure Interaction in Strong Motion Network Stations in Greece, Research Project [8048 RC of AUTH], Final Report Site:Edessa, pp.156 (in Greek).

Fäh, D., Kind, F. and Giardini, D., 2001, A theoretical investigation of average H/V ratios. Geophysical Journal Int., 145, 535-549.

Fäh, D., Kind, F., Giardini, D., 2003. Inversion of local S-wave velocity structures from average H/V ratios, and their use for the estimation of site-effects. Journal of Seismology, 7, 449-467.

ITSAK-Gazetas, 2003, Liquefaction Risk Assessment and Kinematic Soil-Pile Interaction Study for the Nestos Bridge of the Egnatia Motorway, Second Issue Report, pp. (in Greek).

Klimis N., Anastasiadis A., Gazetas G. and Apostolou M., 2004, Liquefaction Risk Assessment and Design of Pile Foundation for Highway Bridge, 13th WCEE, paper No.2973, Vancouver, Canada.

Pitilakis K., Margaris V., Lekidis V., Theodulidis N. and Anastasiadis A., 1992, The Griva, northern Greece earthquake of December 21, 1990. (Seismological, structural and geotechnical aspects), European Earthq. Engin., 2, 20-35.

Satoh, T., Kawase, H., Iwata, T. Higaski, S., Sato, T., Irikura, K. and Huang, H. C., 2001, S-wave velocity structure of Taichung basin, Taiwan estimated from array and single-station records of microtremors, Bull. Seism. Soc. Am. 91, 1267-1282.

Yamanaka, H., Takemura, M., Ishida, H. and Niea, M., 1994, Characteristics of long-period micro-tremors and their applicability in exploration of deep layers, Bull. Seism. Soc. Am. 84, 1831-1841.

3.2. Comparison of the (H/V) spectral ratio with theoretical 1D & 2D approach

Introduction

I this sub-chapter results of site effects based on ambient noise measurements in the city of Thessaloniki, Northern Greece, and in the city of Kalamata, Southern Greece in comparison with results of theoretical approach are described. The work has been accomplished in the following steps including, (I) comparison between the results of ambient noise synthetics and real data at three sections in the historical center of the city of Thessaloniki (for this reason additional measurements were made), (ii) comparison with 1D and 2D synthetic seismograms at selected sites in the historical center of the city of Thessaloniki, (iii) comparison between the results results of ambient noise synthetics and real data at the center of the city of Kalamata. These steps are presented below along with discussion/conclusions regarding evaluation of the applied methodology.

3.2.1(a). Ambient Noise Synthetics for the city of Thessaloniki using Hisada 1D approach.

The computer code used for the noise simulation is composed of two separate Fortran programs (Cornou et al., 2003). In the first one, named "**RANSOURCE**", point sources are generated randomly in space, time, and amplitude according to Moczo and Kristek (2002) following some user-defined criteria. Its output is stored in a file which serves as input for the second program, named "**HISADA**" (Hisada, 1994), which propagates the seismic waves emitted by this set of noise sources in a 1D horizontally layered, hetereogeneous, viscoelastic structure with a planar free surface, and computes the resulting ground motion at a number of predefined receivers (points). Finally, the synthetic noise at each receiver (point) is obtained by the total summation of synthetic recordings that were radiated from each source to the specified receiver (point).

Thereafter, the spectrum of each component of the ambient noise synthetics was calculated first. Then, at each point (receiver) the horizontal record spectrum was divided by the vertical one and the (H/V) spectral ratio was obtained. Finally, the (H/V) spectral ratio was plotted versus frequency and the theoretical fundamental frequency was defined visually at each point (receiver).

Three sections covering different geological conditions of the city of Thessaloniki (IGME, 1978) were chosen as an example to demonstrate and check the (H/V) spectral ratios results of ambient noise synthetics.

The first section is shown in Figure 1 and is parallel to the coastline. The simulated noise, computed at nine receivers (points), is emitted by 300 random sources in space, time occurence, maximum amplitude and body force acting direction. The position of the sources in relation with the receivers is shown in the upper part of Figure 2. The geotechnical model (Anastasiadis et al., 2001), that describes the layering of the formation of the section is illustrated in the lower part of Figure 2. Figure 3 shows the fundamental frequencies that were estimated from the (H/V) spectral ratios of noise synthetics versus the location of the site in this section (see Fig.1 to locate points). As can be seen the estimated fundamental frequencies of the noise synthetics in all nine points (receivers) have comparable values. This observational result was expected because the geological units are not very different along the section. The comparison between the fundamental frequencies that were calculated from noise synthetics and those calculated from microtremor measurements are in good agreement at every point (receiver) of this section.

The second section is shown in the upper part of Figure 4 and is perpendicular to the coastline (Ethnikis Aminis). Additional measurements were made at this section in order to have at least 50m distance between examined points. As it appears, (lower part of Figure 4) the soil stratigraphy of this section is more complex forming a 2D or even 3D medium (Pitilakis et al., 2003). Since the "**HISADA**" code geotechnical input consists of 1D horizontal layers, we divided the section into three parts, so that in each one of them the subsoil stratigraphy is almost horizontally layered. The first part of Ethnikis Aminis is between points 1 to 7, the second part is between points 8 to 14 and the third part is between points 15 to 21. The simulated noise, computed at twenty-one receivers (points), is emitted by 300 random sources (in space, time occurence, maximum amplitude and body force acting direction). The position of the sources in relation with the receivers is shown in Figure 5. For the three parts of Ethnikis Aminis the different geotechnical models (Anastasiadis et al., 2001), are illustrated in Figure 6. Figure 7 shows the fundamental frequencies that were estimated from the (H/V) spectral ratios of noise synthetics versus the location of the site in this section (see Fig.4 to locate points). Examining the values of fundamental frequencies of the noise synthetics it can be realized that they are increasing with an increase in distance from the shoreline, which is interpreted as a thickening of the alluvial depositstowards the coastline. Regarding the comparison between the fundamental frequencies that were calculated from noise synthetics with those from microtremor measurements. It seems that their values between points (receivers) 8 to 21 are in very good agreement. However, for points (receivers) 2 to 7 there is a slight divergence among them, that is most probably due to lack of a detailed geotechnical model especially in surficial layers.

The third section is shown in Figure 8 and is perpedicular to the coastline. The simulated noise, computed at seven receivers (points), is also emitted by 300 random sources in space, time occurence, maximum amplitude and body force acting direction. The position of the sources in relation with the receivers is shown in the upper part of Figure 9. The geotechnical model (Anastasiadis et al., 2001), that describes the layering of the formation of the section is illustrated in the lower part of Figure 9. Figure 10 shows the fundamental frequencies that were estimated from the (H/V) spectral ratios of noise synthetics versus the location of the site in this section (see Fig. 8 to locate points). As can be seen the estimated fundamental frequencies of the noise synthetics in almost all points (receivers) have comparable values. Only for point 3 there is a divergence between experimental and theoretical estimation of the order of 25%. The comparison between the fundamental frequencies that were calculated from noise synthetics and those calculated from microtremor measurements are in good agreement fot the examined section.

3.2.1(b). Comparison of experimental H/V spectral ratio with 1D & 2D Synthetics

To check the applicability of our analysis to estimate the site fundamental frequency and amplitude, we compared our H/V spectral ratios results with the available geotechnical data of Thessaloniki. For this purpose five sections (directions A, B, C, D and E upper part of Figure 11) covering different geotechnical conditions of the city (Anastasiadis et al., 2001) are chosen as an example. Using the velocity and layer thickness values from Anastasiadis et al., (2001), we have calculated the corresponding fundamental frequencies, using the algorithms proposed by Kanai (1962) and Hadjian (2002). Figures 11 (Lower part) shows the estimated fundamental frequencies from the H/V spectral ratios versus the location of the site at each section (see upper part of Fig. 11

to locate points). As can be seen, the estimated fundamental frequencies by all examined methods are in very good agreement with those estimated by the H/V spectral ratio from ambient noise measurements.

To further validate our results, H/V spectral ratios were compared with the transfer functions obtained considering the one-dimensional (1-D) propagation of vertically incident SH waves (Kennett and Kerry, 1979). Using the geotechnical information from Anastasiadis et al. (2001) SH-waves transfer functions were calculated for four sites in the center of the city (Figure 12). Comparison of the experimental ambient noise H/V spectral ratios with numerical ones reveals a good overall agreement. Although the amplification obtained by the ambient noise H/V spectral ratio is generally lower than that obtained by the numerical modeling, the fundamental frequency of each site is similar for both methods. Furthermore, except from site CIT, ambient noise H/V spectral ratio did not give any information on the higher harmonics of the fundamental frequency.

Tiantafyllidis et al., (2002) used seven douple-couple points sources located at different epicentral distances and azimuths from the city of Thessaloniki to produce synthetic acceleration wavefield for all components of motion. For four sites in the center of the city (Figure 13) we compared the experimental ambient noise H/V spectral ratios with those of the 2-D accelerometer synthetics. Such a comparison is shown in Figures 14 to 17 for the frequency band 0.5 to 6 Hz (Triantafyllidis et al., 2002). In general, the results show that there is a similarity for all sites in the overall shape of the H/V spectral ratio obtained by the two different techniques. At AGO and ROT we could not observe the fundamental frequency of the sites because in the 2D simulation maximum cutoff frequency is 6 Hz. More importantly, there is a good agreement on the determination of the fundamental frequency of CIT and LEP.

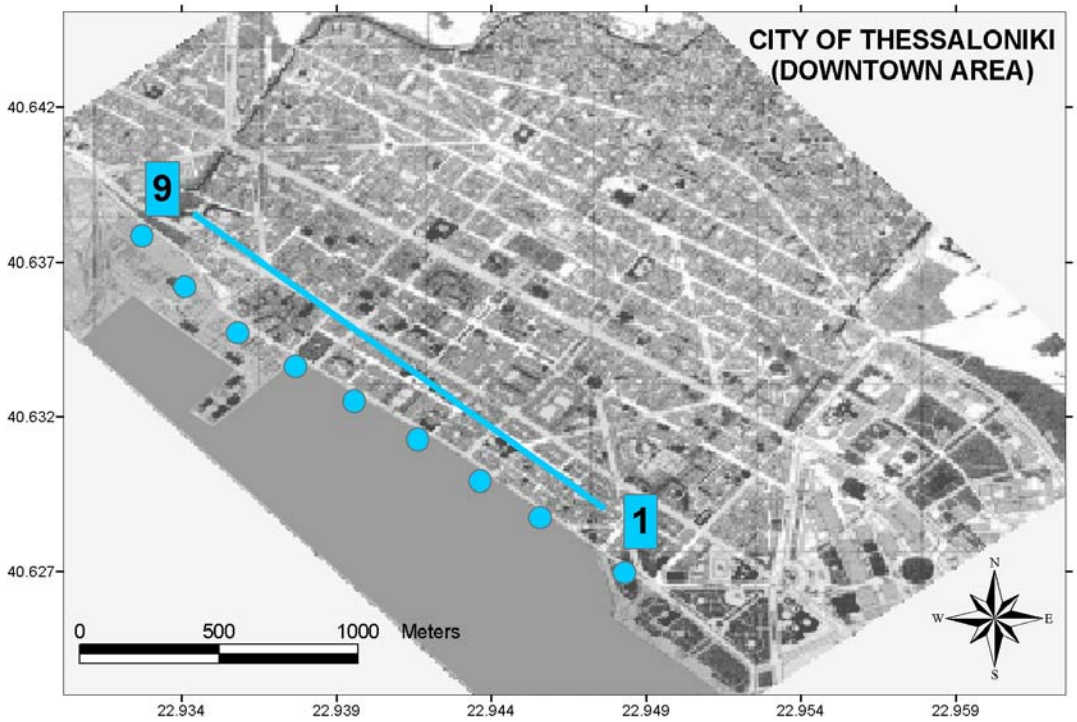

Figure 1: Location of the points (receivers) in the section that is parallel to the coastline where ambient noise synthetics were calculated.

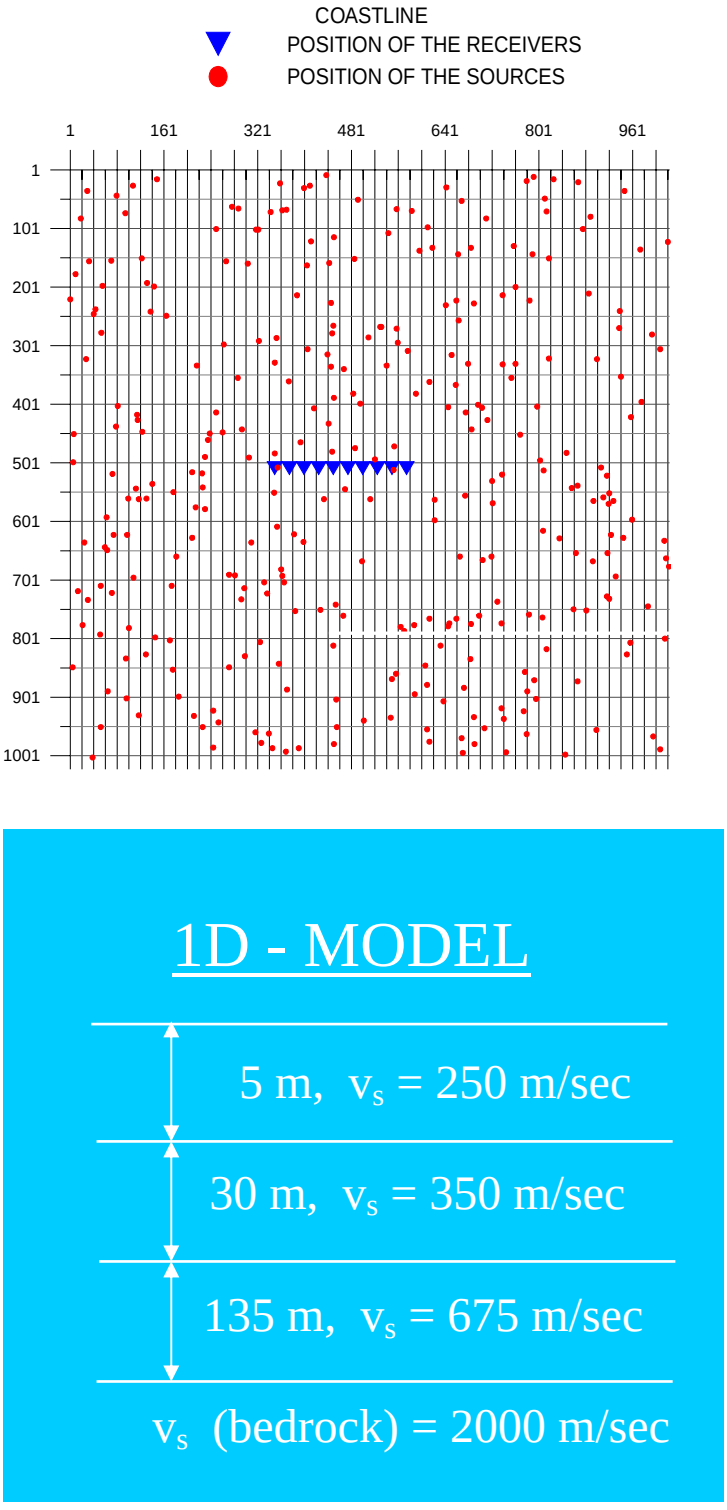

Figure 2: *Upper part:* Position of the sources in relation with the receivers (points) in the section parallel to the coastline. *Lower part:* Geotechnical model of the section (Anastasiadis et al., 2001).

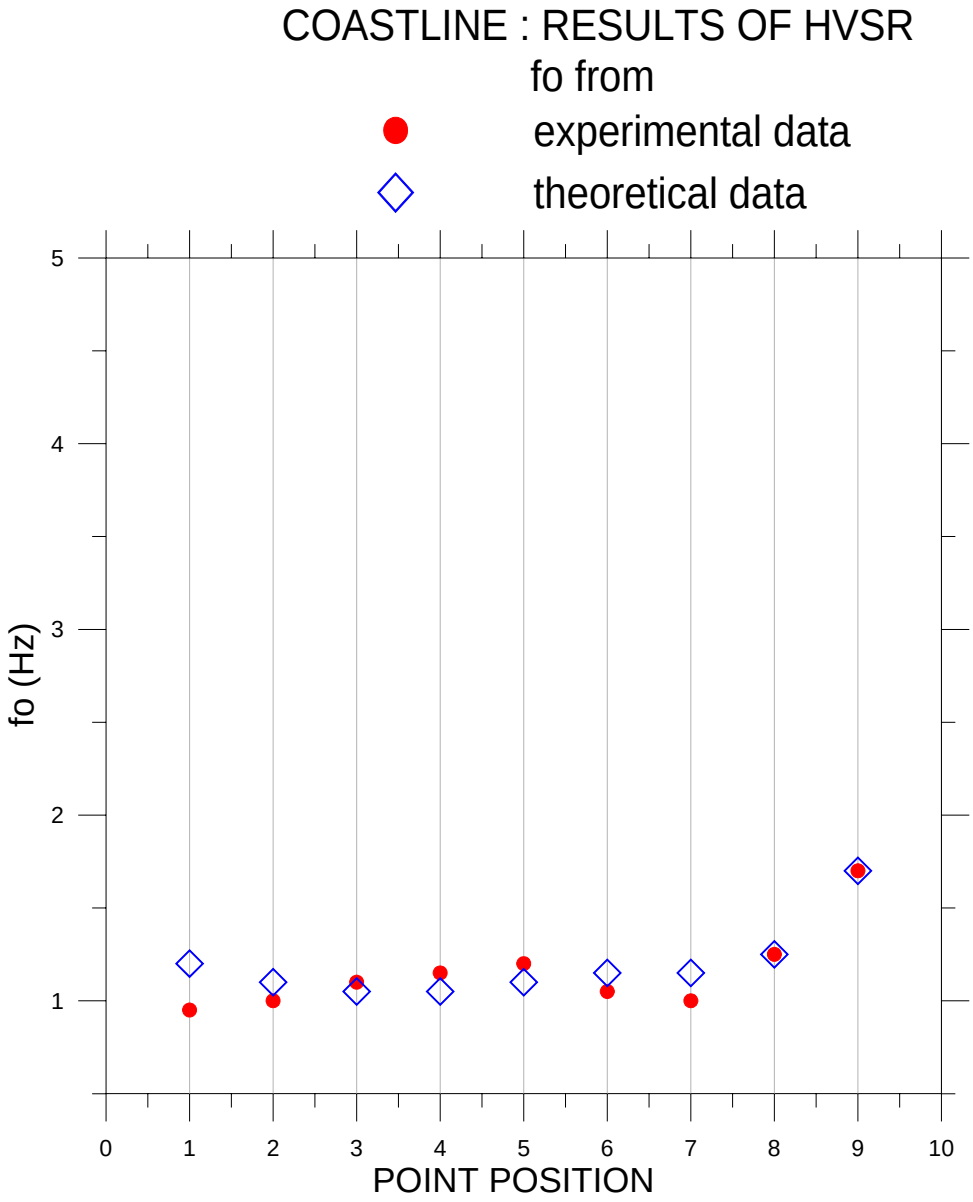

Figure 3: Fundamental frequencies versus the location of the point (receiver) for the section that is parallel to the coastline.

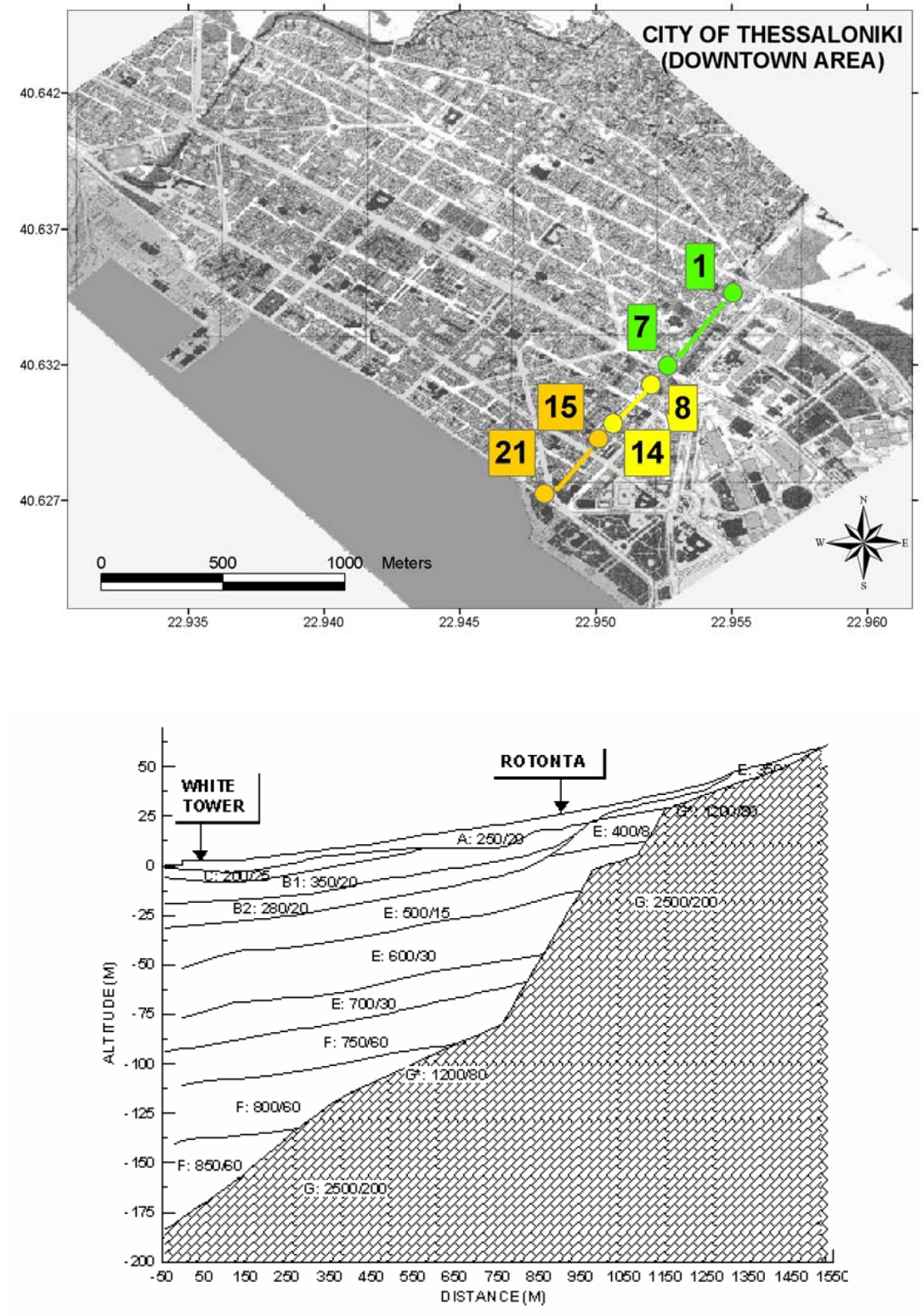

Figure 4: *Upper part:* Location of the points (receivers) that ambient noise synthetics were calculated. *Lower part:* Geotechnical information of the section (Pitilakis et al, 2003).

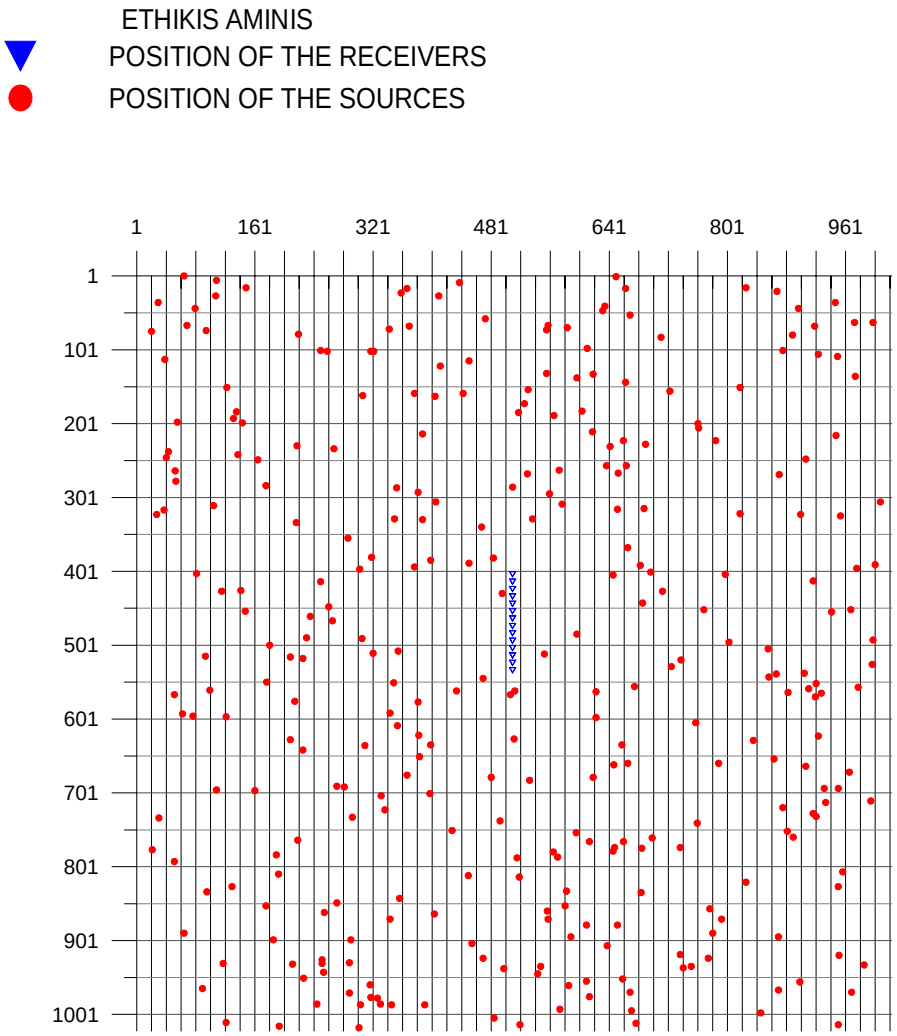

Figure 5: Position of the sources in relation with the receivers (points) in the section.

1D - MODEL

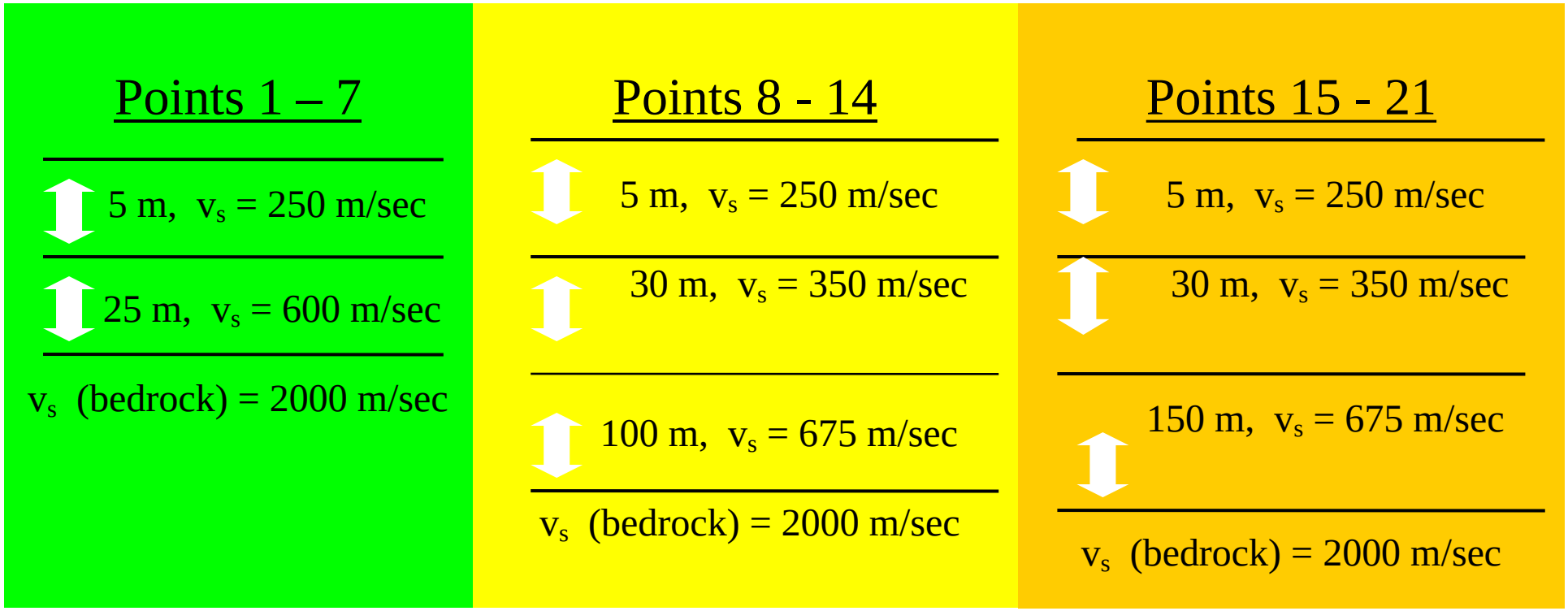
Points 1 – 7
5 m, v_s = 250 m/sec
25 m, v_s = 600 m/sec
v_s (bedrock) = 2000 m/sec
Points 8 - 14
5 m, v_s = 250 m/sec
30 m, v_s = 350 m/sec
100 m, v_s = 675 m/sec
v_s (bedrock) = 2000 m/sec
Points 15 - 21
5 m, v_s = 250 m/sec
30 m, v_s = 350 m/sec
150 m, v_s = 675 m/sec
v_s (bedrock) = 2000 m/sec

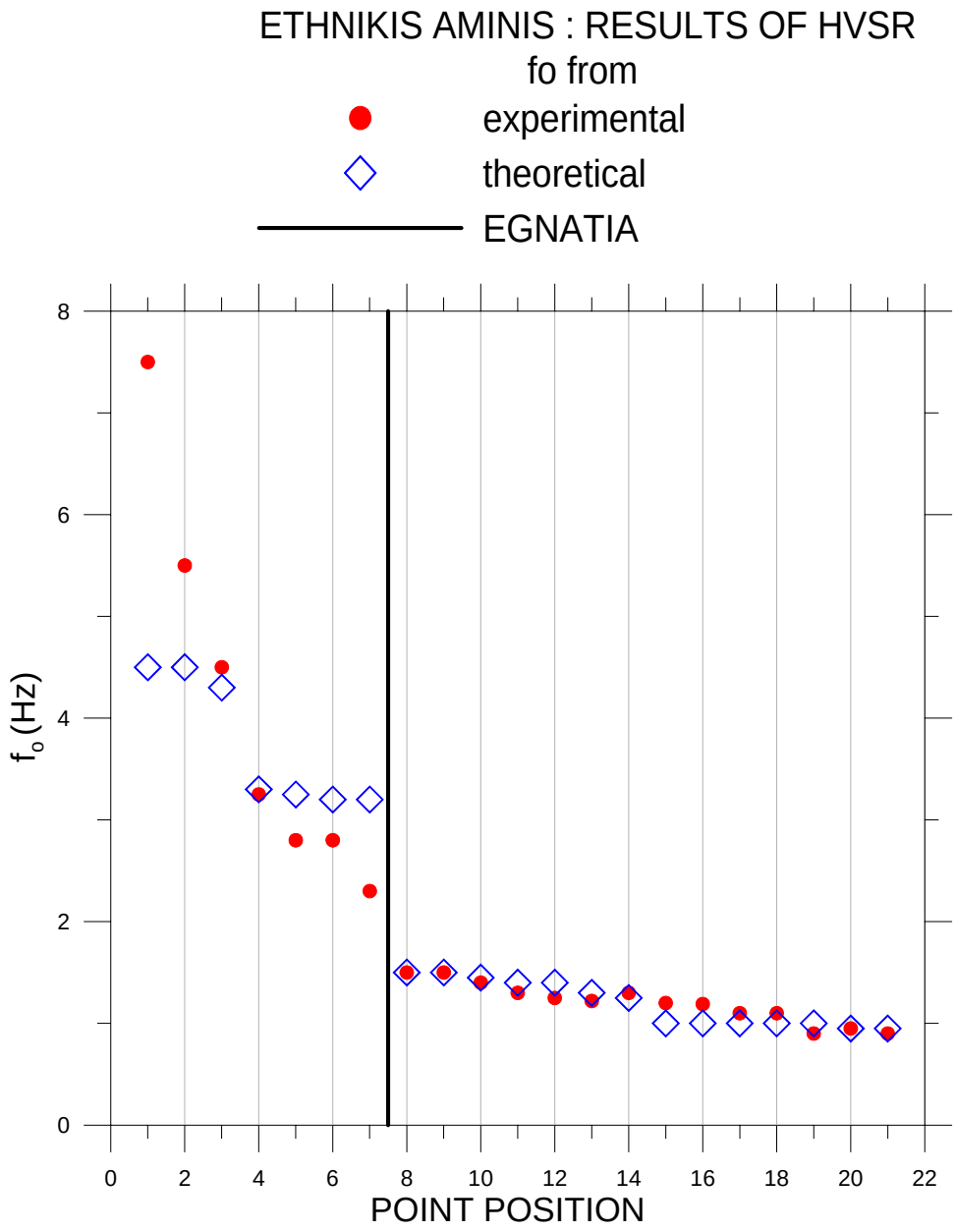

Figure 7: Fundamental frequencies versus the location of the point (receiver) for the Ethnikis Aminis section.

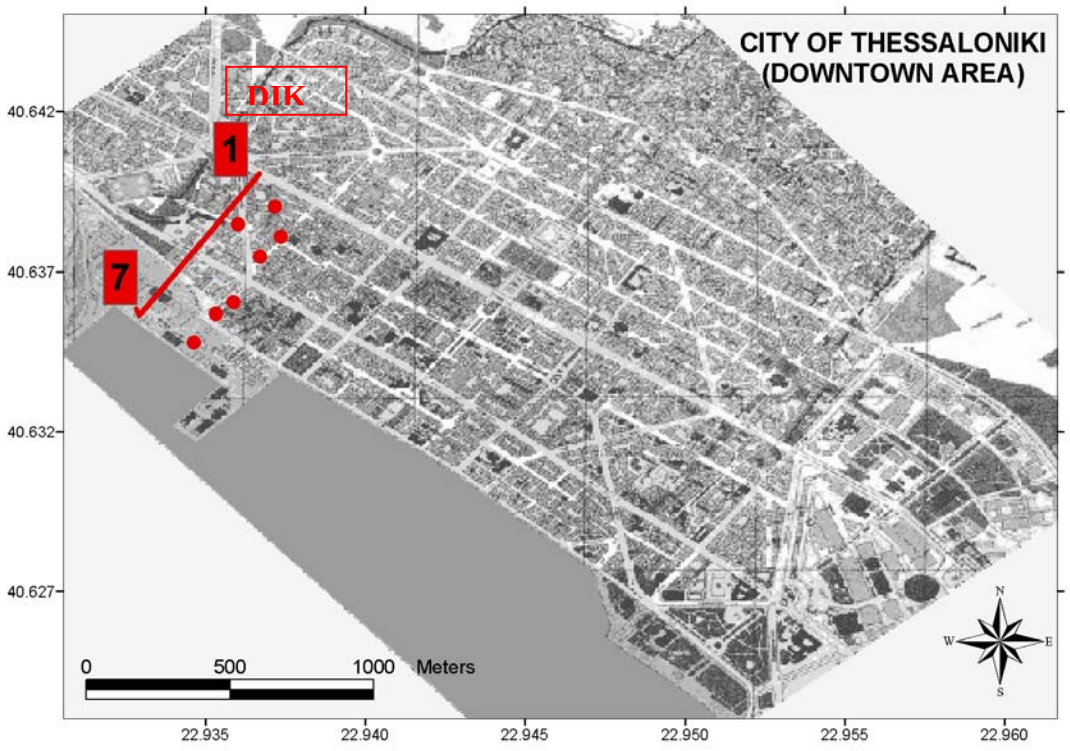

Figure 8. Location of the points (receivers) that ambient noise synthetics were calculated (section DIK).

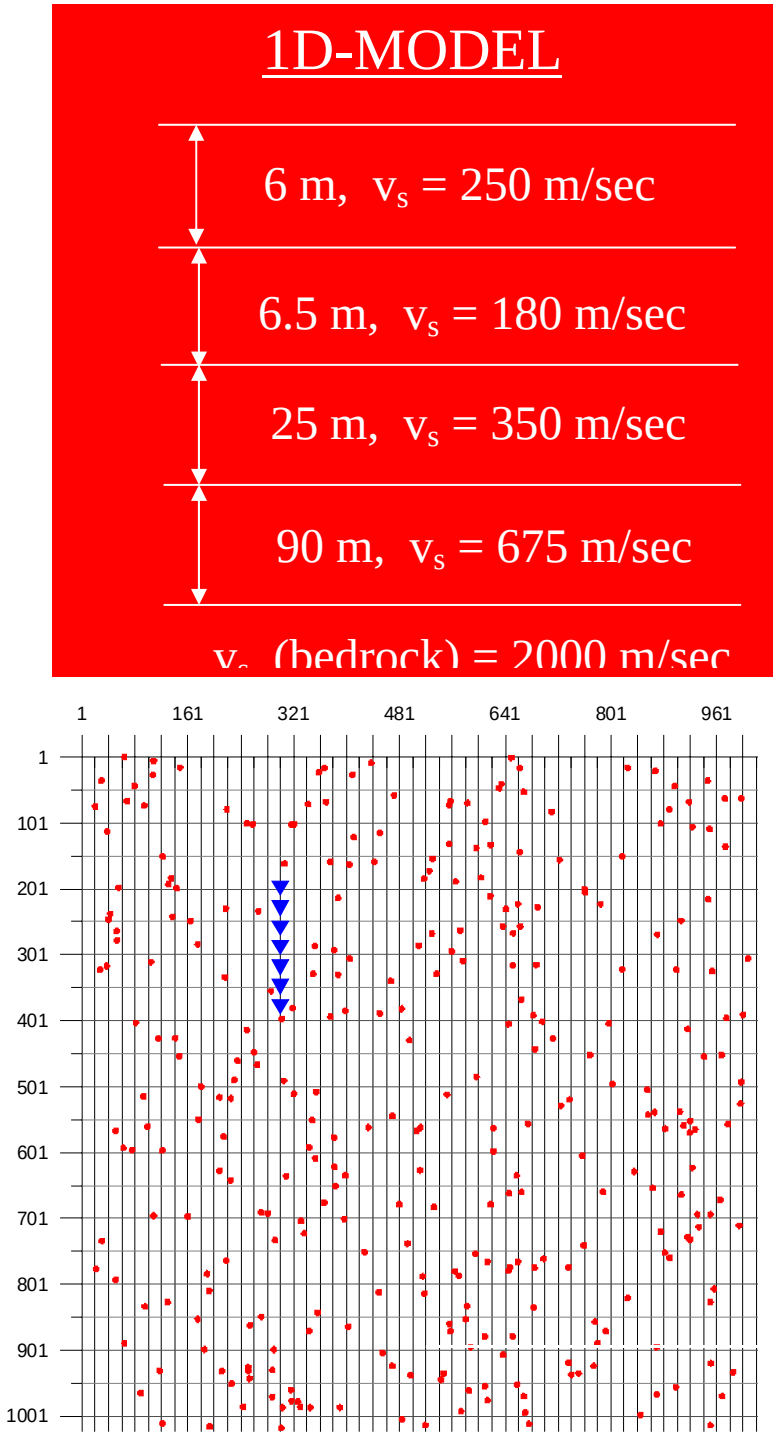

Figure 9. *(Upper part)* Geotechnical model of the DIK section (see Fig. 8). *(Lower part)* Position of the sources in relation with the receivers (points) in the section DIK.

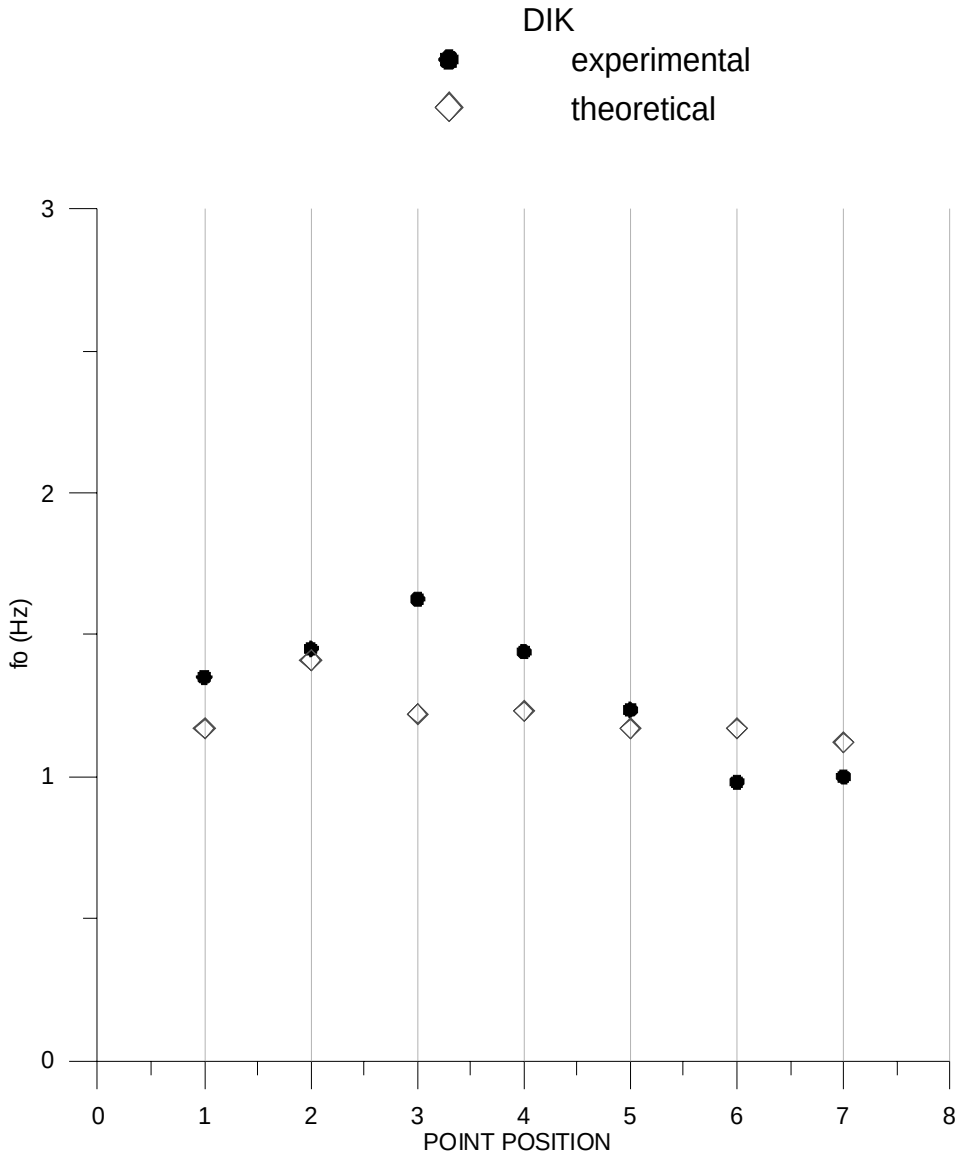

Figure 10. Fundamental frequencies versus the location of the point (receiver) for the DIK section.

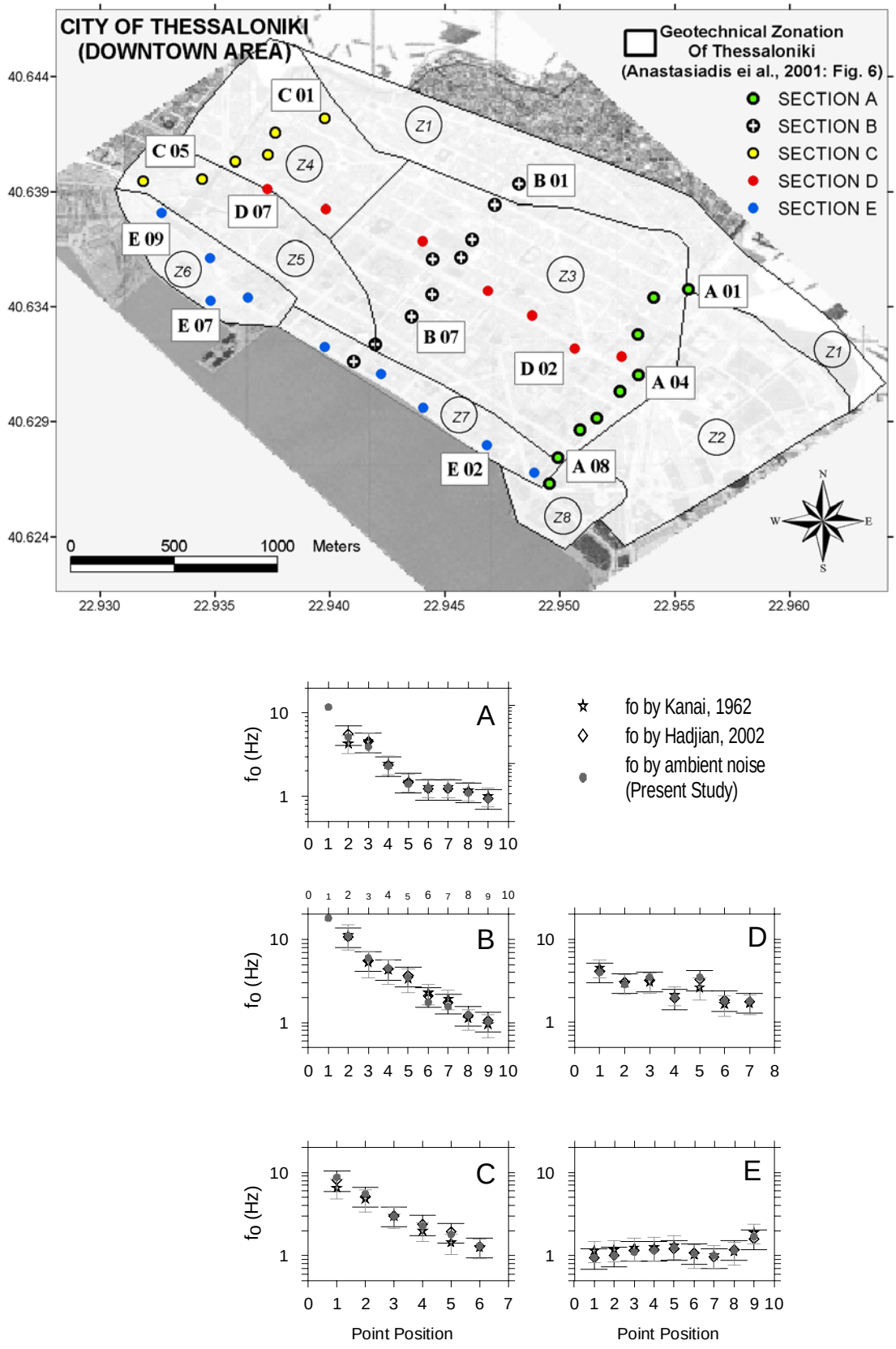

Figure 11. **(***Upper part)*: Location of ambient noise recording points in sections A, B C, E and D. *(Lower part)*: Fundamental frequencies variation along each cross-section.

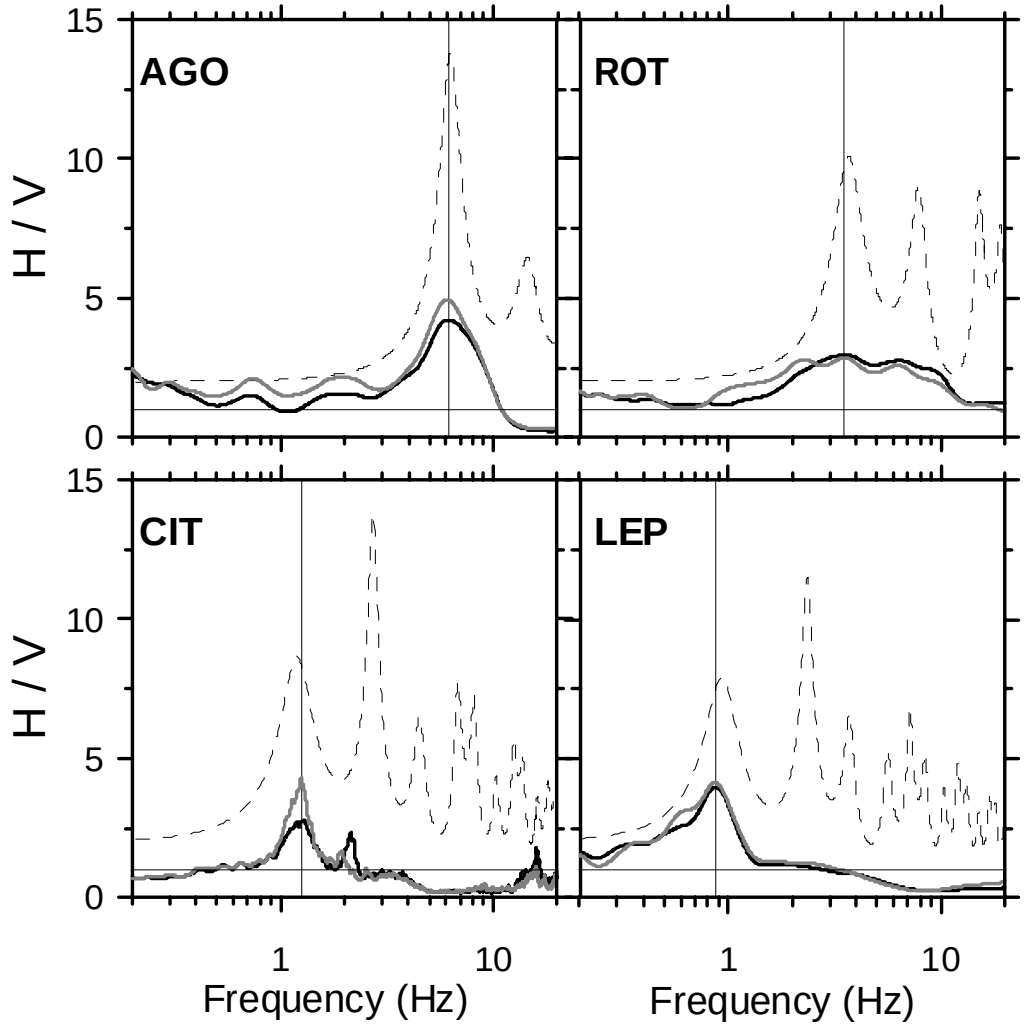

Figure 12. Comparison of experimental H/V spectral ratios (solid lines) with SH-waves 1D transfer functions (dashed line) for four examined sites in the city of Thessaloniki (see Fig. 13).

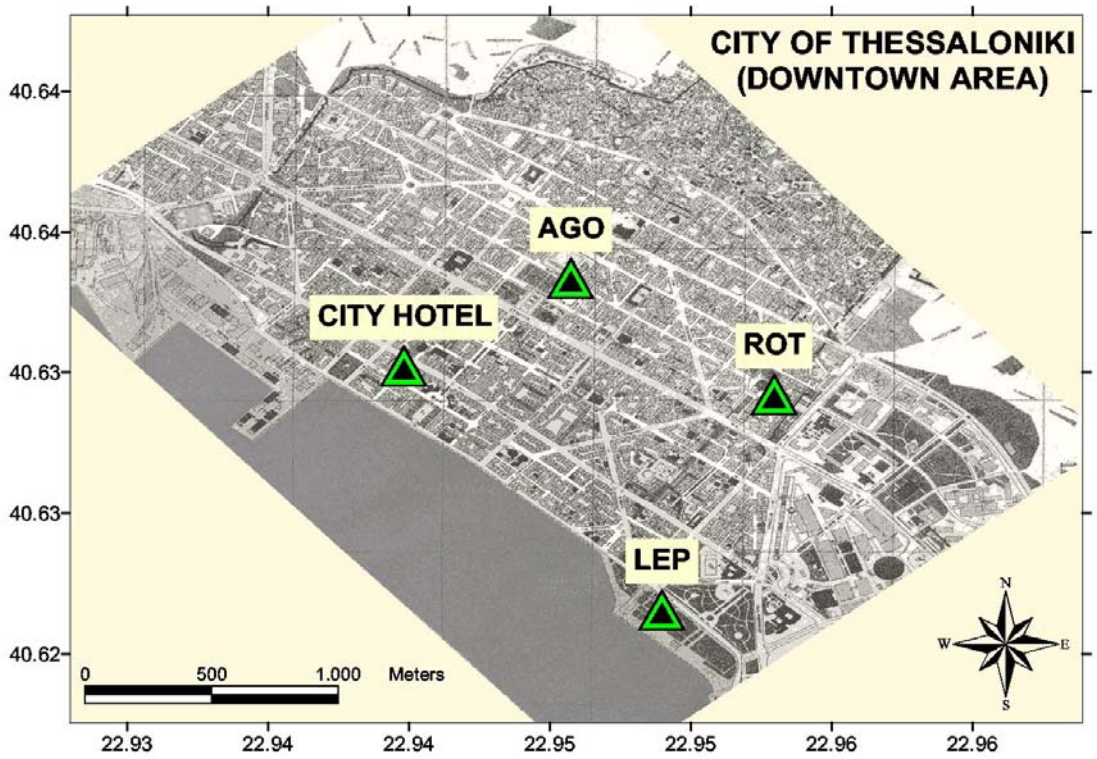

Figure 13. Location of the sites of the 2D accelerometer synthetics in the city of Thessaloniki.

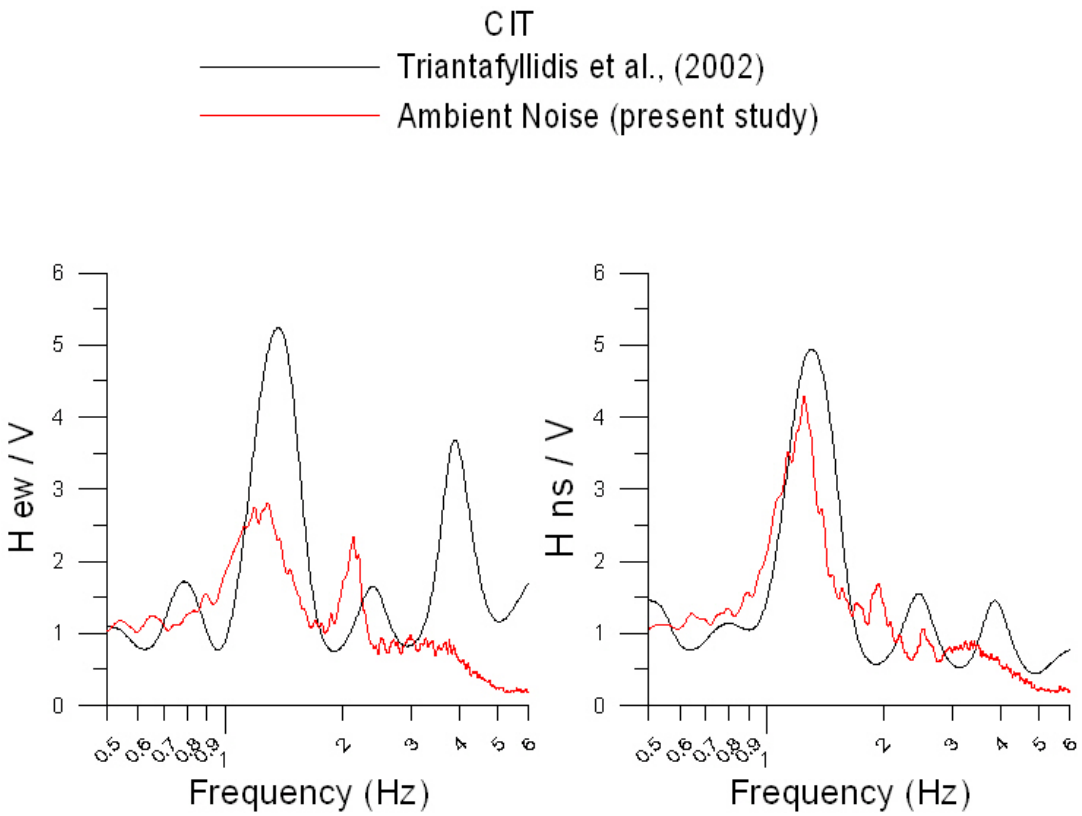

Figure 14.

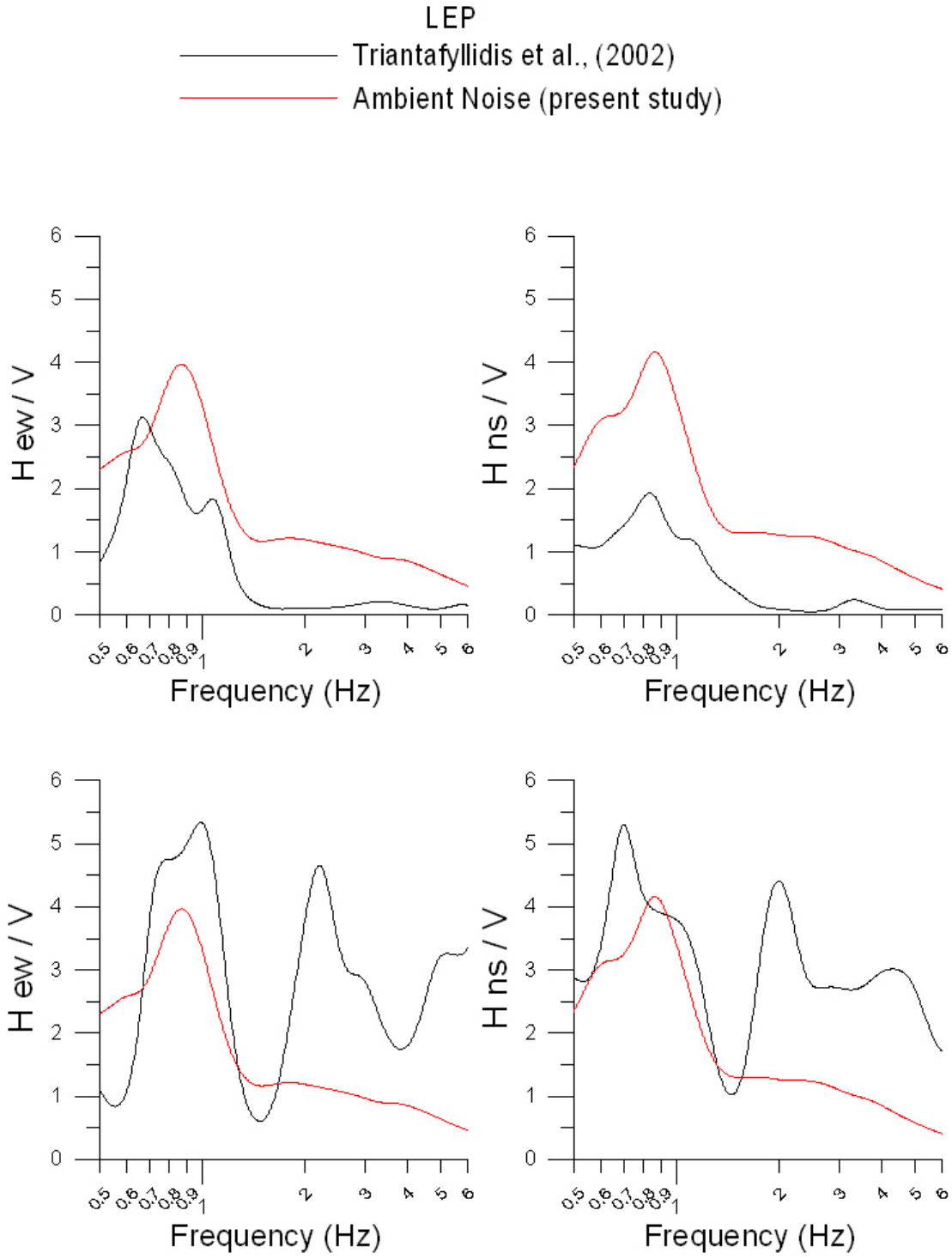
LEP
Triantafyllidis et al., (2002)
Ambient Noise (present study)
H ew / V
H ns / V
Frequency (Hz)
0.5
0.6
0.7
0.8
0.9
1
2
3
4
5
6
0
1

Figure 15.

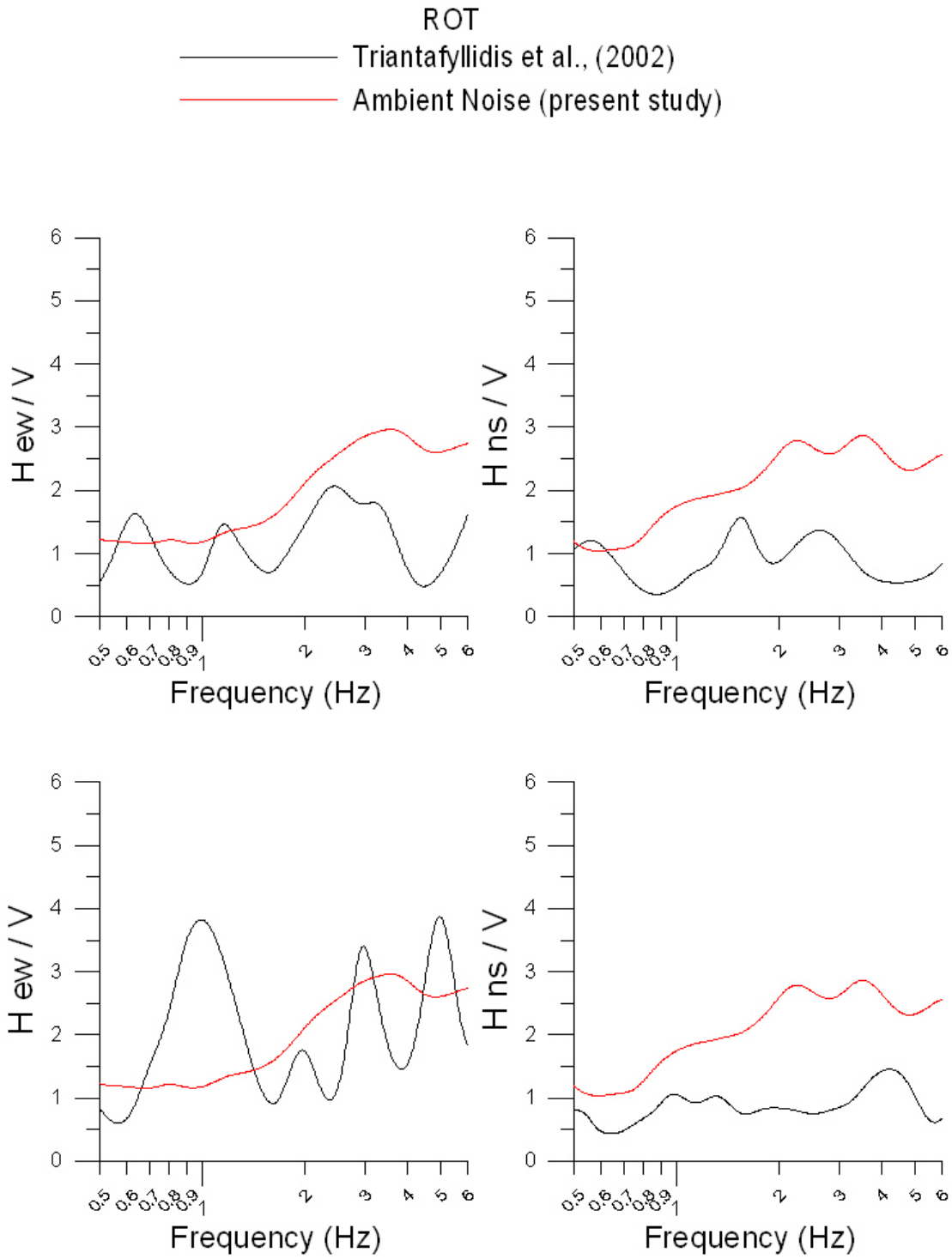
ROT
Triantafyllidis et al., (2002)
Ambient Noise (present study)
H ew / V
H ns / V
Frequency (Hz)
0.5
0.6
0.7
0.8
0.9
1
2
3
4
5
6
0
1
2
3
4
5
6

Figure 16.

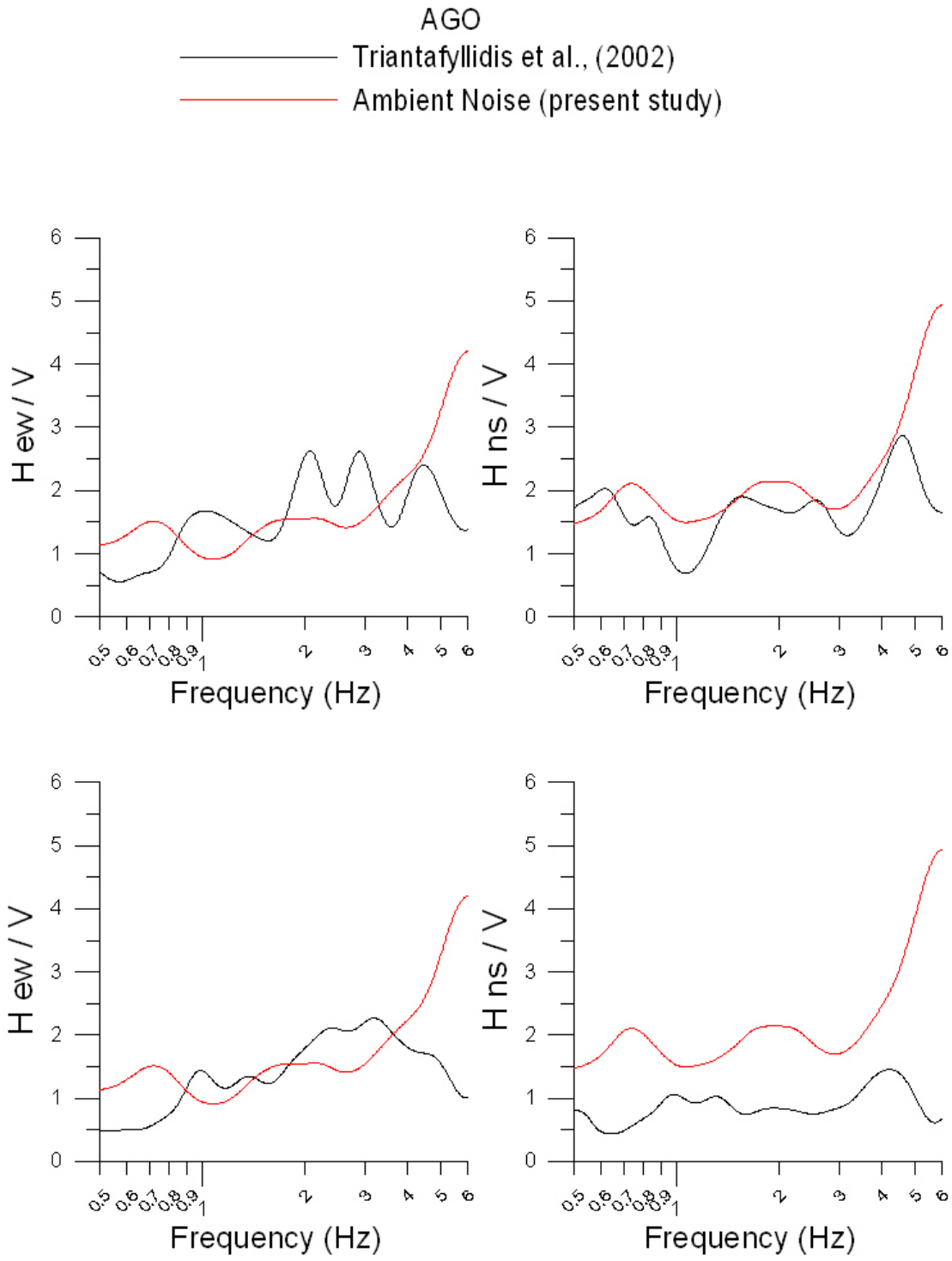

Figure 17

Figures 14-17: Comparison of the experimental ambient noise H/V spectral ratio (red line) with corresponding spectral ratio of 2D accelerometer synthetics (Triantafyllidis et al., (2002); (black line).

3.2.2. Ambient Noise Synthetics for the City of Kalamata

Ambient noise measurements were also performed in the city of Kalamata (Southern Greece) (Figure 18) in a grid covering almost the whole city. The recordings were preformed late in the evening, from Monday to Friday. The equipment used comprises the Cityshark recorder 24-bits recorder (Chatelain et al., 2000) coupled with a Lennartz 3D/5s velocimeter sensor. A GPS system provided the geographic position of each measurement point. In the experiment, the recording system operated continuously for 20 min. The sample rate was 100 Hz.

Ambient noise data were processed in two stages. First, for each ambient noise recording, a number of windows, having a duration of 20 sec each, were selected using the 'winselect' code of the JSESAME software (SESAME project, 2003), in order to exclude portions with forbiddingly large amplitudes or spikes, as has been suggested by Duval et al., (2003). To these data, using the 'hvproc' code of the JSESAME software (SESAME project, 2003), the following processing was made: (a) computation of Fourier spectra in all three components (E–W, N–S, UP), (b) offset correction, (c) application of a cosine taper, (d) smoothing of the Fourier spectra by the Konno-Ohmachi routine (Konno and Ohmachi, 1998). For each point the horizontal record spectrum was divided by the vertical one and the H/V spectral ratio were obtained. The second step consists of plotting ambient noise H/V spectral ratio versus frequency. Each measurement point provides a spectral ratio and enables an estimation of the fundamental frequency (fo) and the maximum value of the ambient noise (H/V) spectral ratio amplitude level (Ao) at the site studied. By spatial interpolation between these points, we can deduce a map of resonance frequencies (fo) and a map of the maximum H/V amplitude level (Ao) observed at these fundamental frequencies. Figures 19(a),(b),(c) present the variation with frequency of the average *H/V* ambient noise spectral ratio for three representative of the center of the city ambient noise recordings. The averaged H/V ambient noise spectral ratios, shown in Figure 19 display a range in complexity (e.g. ranging from two to three peaks). The character of the H/V ambient noise spectral ratios might be related either to the subsurface topography or to geological layers variety idicaring more than one interfaces with high impedance contrast.

Such variation. researchers has been also observed by several researchers. Luzón et al., (2001), studied the seismic response of flat sedimentary basins and carried out numerical experiments to determine the applicability of the H/V ambient noise spectral ratio in two different kinds of structure. They concluded that H/V ambient noise spectral ratio could, reasonably well, predict the fundamental local frequency when there is a high-impedance contrast between the sedimentary basin and the bedrock, except in the center of the basin. On the other hand H/V ambient noise spectral ratio could not be used, at least in sedimentary basins with low-impedance contrast with respect to bedrock. Cid et al., (2001), studied the seismic response of different sites of Barchelona through numerical modeling. Their numerical results compared with those obtained from ambient noise measurements and showed that H/V ambient noise spectral ratio predicts the fundamental frequency of the site only when there is a sharp shear-wave velocity interface in the soil column. Woolery and Street (2002), observed that a relatively horizontal, sharp shear-wave velocity interface in the soil column resulted in an H/V ambient noise spectral ratio with a single well-defined peak in the New Madrid seismic zone in the central United States. Observations at sites with more than one sharp shear-wave velocity contrast and horizontally arranged soil layers resulted in at least two well-defined H/V ambient noise spectral ratio peaks. Furthermore, at sites where there were sharp shear-wave velocity contrasts in nonhorizontal, near-surface soil layers, the H/V ambient noise spectra exhibited a broad-bandwidth, relatively low amplitude signal instead of a

single well-defined peak. The city of Kalamata divided in two categories with respect to fundamental frequencies: one with fo > 1 Hz and another with fo <1 Hz.

Theoretical 1D ambient noise synthetics - using the Hisada code and geotechnical model of Table 1 - estimated for the center of the city of Kalamata and their H/V spectral ratio is given in Figure 20. Comparison of theoretical with the corresponding H/V experimental spectral ratios (Figs. 19) exhibit a good agreement with respect to estimated fundamental frequencies, encouraging thus further research.

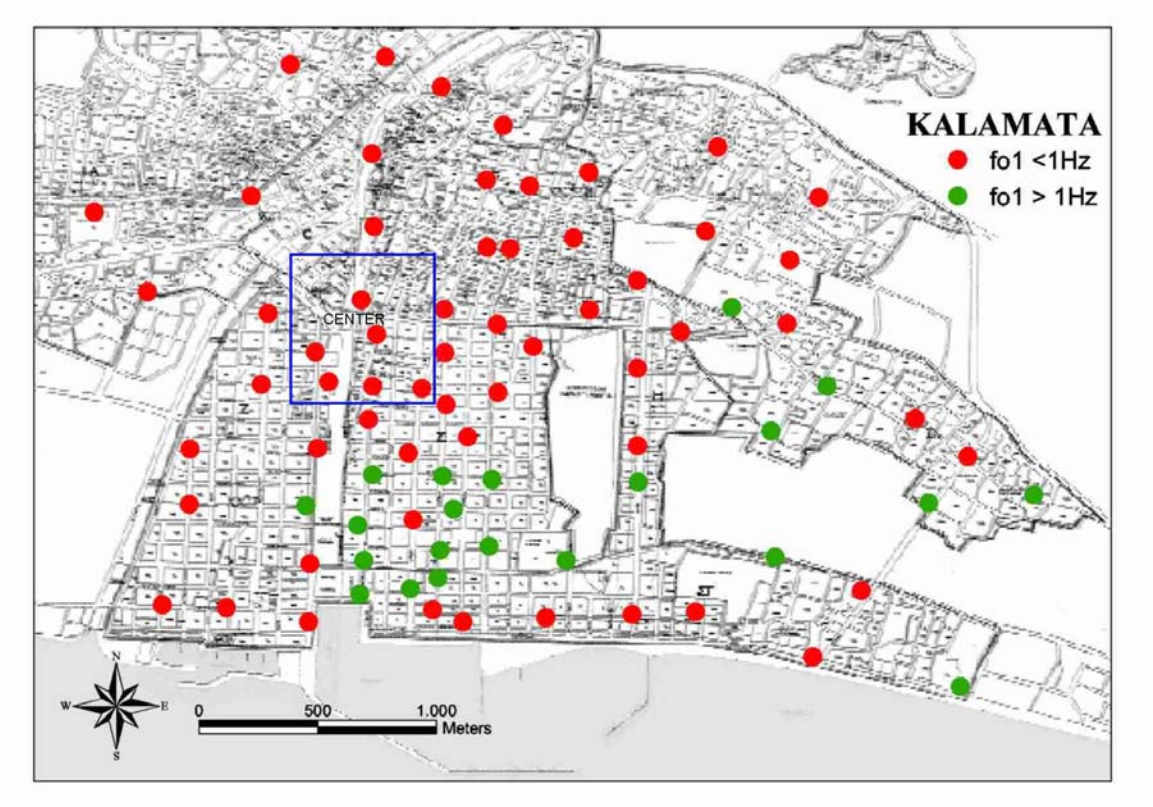

Figure 18. Map of the city of Kalamata along with the point measurement of ambient noise.

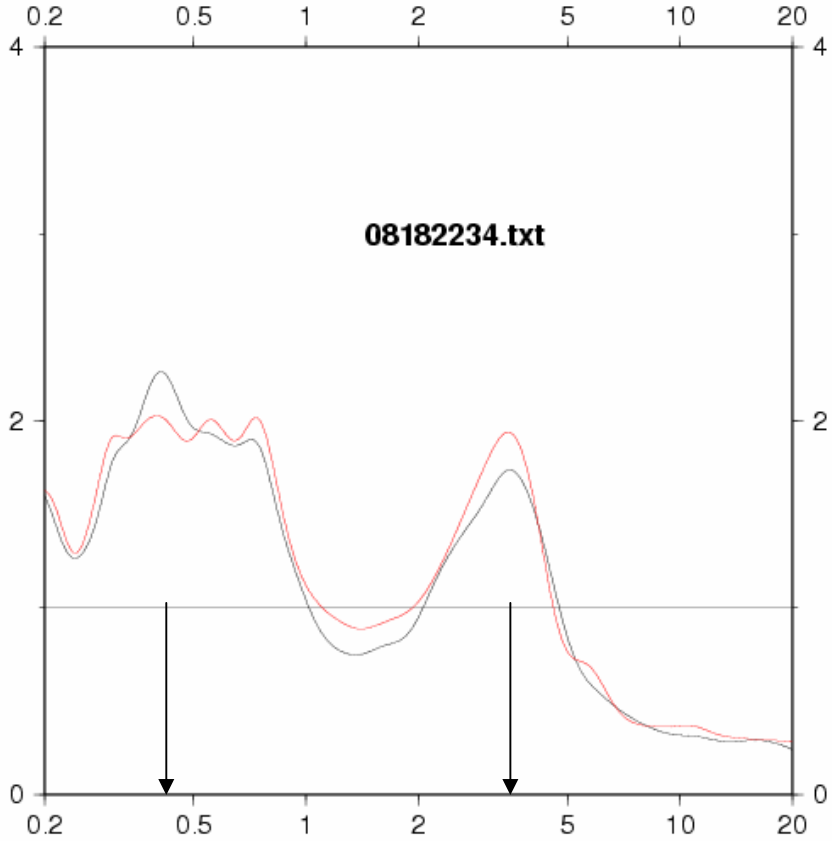

Figure 19 (a).

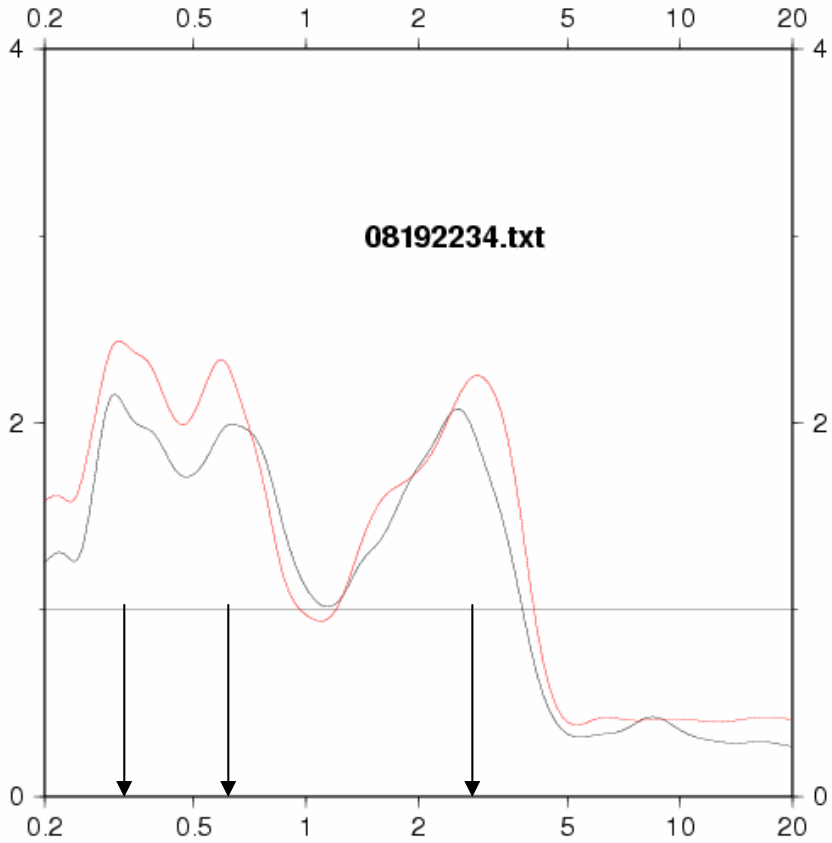

Figure 19 (b)

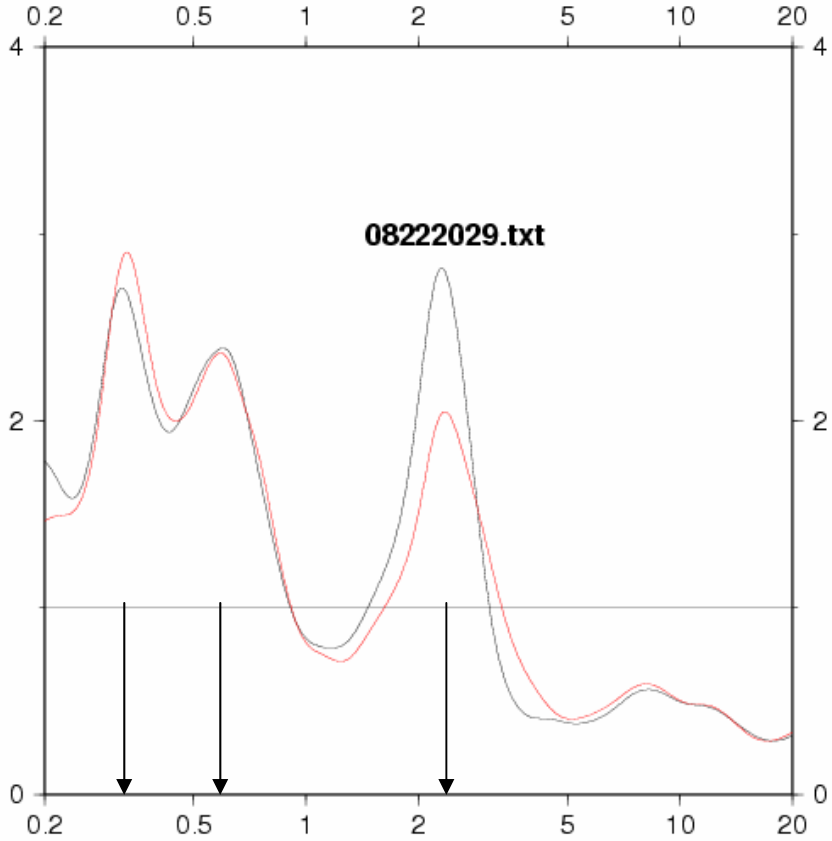

Figure 19 (c)

Figures 19(a),(b),(c). Plots of the average H/V spectral ratio versus frequency for three measurement points representative of the center of Kalamata. (*Red line*: east-west component, *Black line*: north-south component).

Table 1. Geotechnical model for the center of the city of Kalamata.

Layer Thickness(m)	Vs(m/sec)	Qs	Density (Kg/m3)	Vp(m/sec)	Qp
11	200	8	1950	1580	380
9	300	10	2000	1460	180
9	500	12	2050	1640	100
2	1000	25	2050	4500	380
180	600	16	2150	1930	125
HS	1100	25	2150	5500	380

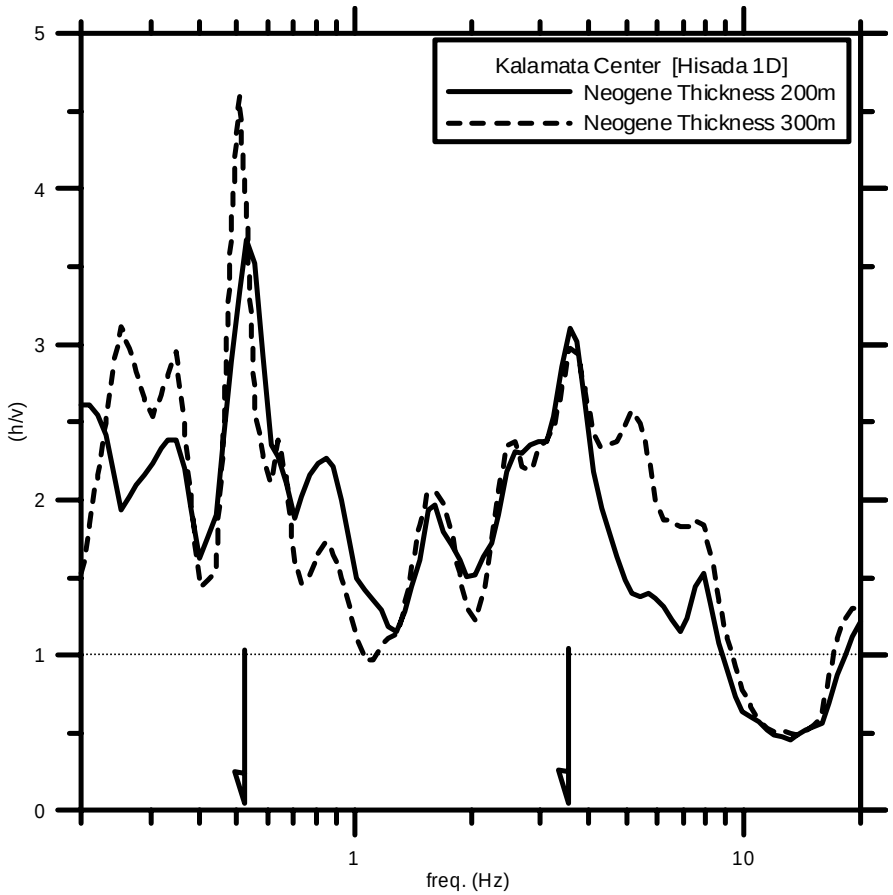

Figure 20. H/V spectral ratio based on synthetic 1D Hisada theoretical approach for the center of the city of Kalamata.

References

Anastasiadis, A., Raptakis, D., Pitilakis, K., (2001). Thessaloniki's Detailed Microzoning: Subsurface Structure Site Response Analysis, *Pure and Applied Geophysics*, 158, 2597 – 2633.

Chatelain, J.-L., Gueguen, Ph., Guillier, B., Frechet, J., Bondoux, F., Sarrault, J., Sulpice, P., and Neuville J.-M. (2000), Cityshark: A user-friendly instrument dedicated to ambient noise (microtremor) recording for site and building response studies, Seismol. Res. Lett. 71, 698-703.

Cid J., Susagna T., Goula X., Chavarria L., Figueras S., Fleta J., Casas A., and Roca, A. (2001), Seismic zonation of Barcelona based on nunerical simulation of site effects, Pure Appl. Geophys. 158**,** 2559-2577.

Cornou, C., Bonnefoy-Claudet, S., Kristek, J., Fäh, D., Bard, P.-Y., Moczo, P., Cotton, F., (2003). Seismic ambient vibrations : what sources for simulating noise?, *Poster at the Assembly of the European Geophysical Society, the American Geophysical Union and the European Union of Geophysicists (E.G.S. - A.G.U. – E.U.G.).*

Duval, A.-M., Chatelain, J.-L., Guillier. B., and the SESAME WP02 team (2003), Influence of experimental conditions on H/V determination using ambient vibrations (noise), 13th World Conference on Earthquake Engineering, 1-6 August, 2004, (Vancouver, British Columbia, Canada) (Submitted).

European Macroseismic Scale, 1998, http://www.gfz-potsdam.de/pb5/pb53/projekt/ems.

Hisada, Y., 1994. An efficient method for computing Green's functions for a layered half-space with sources and receivers at close depths, *Bull. Seism. Soc. Am.*, 84, 5, 1456-1472.

IGME, (1978). Geological map of Thessaloniki, *Institute of Geology and Mineral Exploration.*

Kennett B., and Kerry N., Seismic waves in a stratified half space, Geophys. J. R. Astr. Soc., 57,557-583, 1979.

Konno, K., and Ohmachi T. (1998). Ground-motion characteristics estimated from spectral ratio between horizontal and vertical components of microtremor, *Bull. Seism. Soc. Am.* 88**,** no. 1, 228–241.

Leventakis G., Lekidis V., Papaioannou Ch., Zacharopoulos S., Tsokas G. and Kiratzi A., "Equal-Intensity contour map for the city of Kalamata due to September 1986 earthquake", Proc. 1st Hellenic Conf. of Earthquake Engin. and Engin. Seismology, 1992; 2:321-330 (in Greek).

Luzón F., Al Yuncha Z., Sánchez-Sesma F. J., Ortiz-Alemán C., (2001), A numerical experiment on the Horizontal to Vertical Spectral ratio in Sedimentary Basins, Pure Appl. Geophys. 158**,** 2451-2461.

Moczo, P. and J. Kristek, 2002, FD code to generate noise synthetics, *SESAME Deliverable D02.09*, 31 pp (http://sesame-fp5.obs.ujf-grenoble.fr).

Penelis G., Stylianidis K., Stavrakakis B., (1985). Statistical evaluation of the response of the buildings in the center of Thessaloniki to the earthquake of 20 June 1978, 12th regional Seminar on Earthquake Engineering.

Pitilakis, K., et al., (2003). Site characterization and site response issues for seismic hazard analyses, *GNDT-MAE-SAFERR (GMS) Conference, 26-28 May 2003, Erice Italy, Seismic Risk in Urban Areas.*

SESAME Project 2001, Site EffectS assessment using AMbient Excitations, http://sesame-fp5.obs.ujf-grenoble.fr.

Triantafyllidis, P., Hatzidimitriou, P., Suhadolc, P., (2002). Influence of source on 2-D site effects, *Geophysical Research Letters*, 29, 13, 1-4.

Woolery E. W., and Street R., (2002), 3D near-surface soil response from H/V ambient-noise ratios, Soil Dyn. Earthq. Eng. 22, 865-876.

Chapter 4: (H/V) spectral ratio and nonlinear site response

4.1. (H/V) spectral ratio and non-linear site response

The last decade or so has witnessed a growing interest in nonlinear site response, triggered by the availability of a large amount of quality strong-motion data from earthquakes such as Loma Prieta (1989), Northridge (1994) and Kobe (1995) and representing diverse site conditions (e.g. Jarpe et al., 1988; Darragh and Shakal, 1991; Field et al., 1997, 1998; Aguire and Irikura, 1997; Beresnev et al., 1998a,b; Hartzell, 1998; Cultrera et al., 1999). Nonlinear effects typically cited are (1) deamplification of strong motion relative to weak motion and (2) the decrease of the effective (resonance) frequency of sediments with increasing shaking intensity. The usual approaches to evidencing nonlinear site effects involve looking for amplitude-dependence in spectral ratios either between sediment and rock surface motions – a technique known as standard spectral ratio, or SSR (Borcherdt, 1970) – or between motions at different depths within the deposit. Yet the two approaches encounter certain practical problems. Thus the SSR technique requires a suitable rock (reference) site in the vicinity of the sediment site of interest. Yet in practice it is difficult to find an appropriate reference site, as "rock" sites often have a response of their own (e.g. Cranswick, 1988; Steidl et al., 1996; Boore and Joyner, 1997). On the other hand, the second approach relies on borehole measurements, which are costly and time-consuming. For these reasons, Dimitriu et al. (1999, 2000) have proposed the use of the (non-reference) horizontal-to-vertical spectral-ratio (HVSR, or H/V) technique to characterize nonlinear site response. The application of the method in diverse seismotectonic and geologic environments has evidenced the two aforementioned basic nonlinear effects (Dimitriu et al., 1999, 2000, 2001; Dimitriu, 2002).

Here we compare H/V spectral ratios at five different sediment sites of ITSAK's permanent strong-motion network where available recordings cover a wide range of ground-motion amplitudes, from very weak (ambient noise) to severe (10-35% g). The five sites and the respective largest earthquakes are listed in Table 1.

Table 1. Events with PGA above 10% g recorded at sites of ITSAK's permanent accelerograph network. Also given is site category according to NEHRP'97.

Event	Date	Lat	Lon	M	PGA (g)	Site category (NEHRP'97)
Argostoli	17/1/1983	37.985	20.155	7.0	0.17	C
Athens	7/9/1999	38.059	23.571	5.9	0.30	C
Kalamata	13/9/1986	37.140	22.134	6.0	0.27	C
Lefkas	4/11/1973	38.755	20.454	5.8	0.50	D
Thessaloniki	20/6/1978	40.732	23.242	6.5	0.15	C

Results

Figures 1 to 5 are comparisons of H/V ratios computed from 5-s windows comprising the strongest part of the recordings of the five earthquakes of Table 1 with, on the one hand, average (+ - one standard deviation) H/V ratios from weaker accelerograph recordings and, on the other hand, average (+ - one standard deviation) H/V ratios from ambient noise recordings.

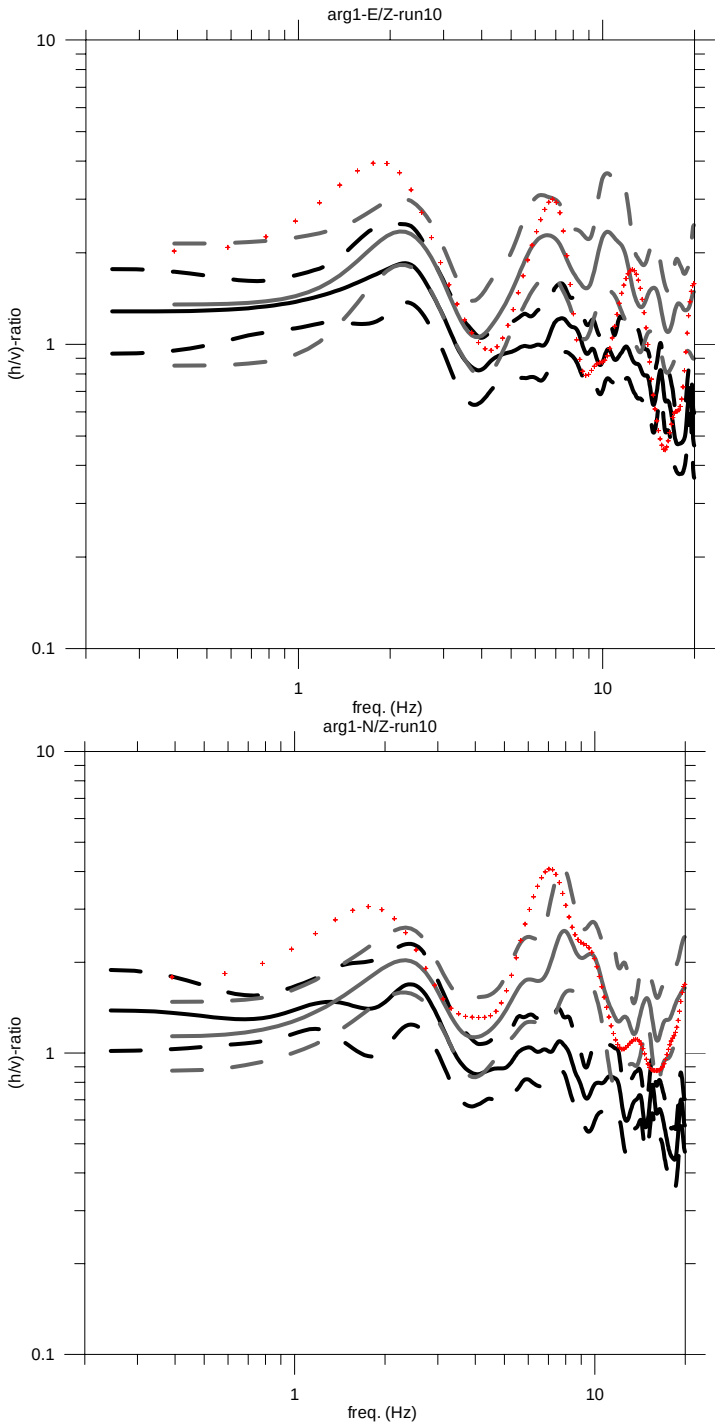

Figure 1. Argostoli site: strong motion (red), weak motion (gray) and ambient noise (black): E-W/Z (upper graph) and N-S/Z (lower graph).

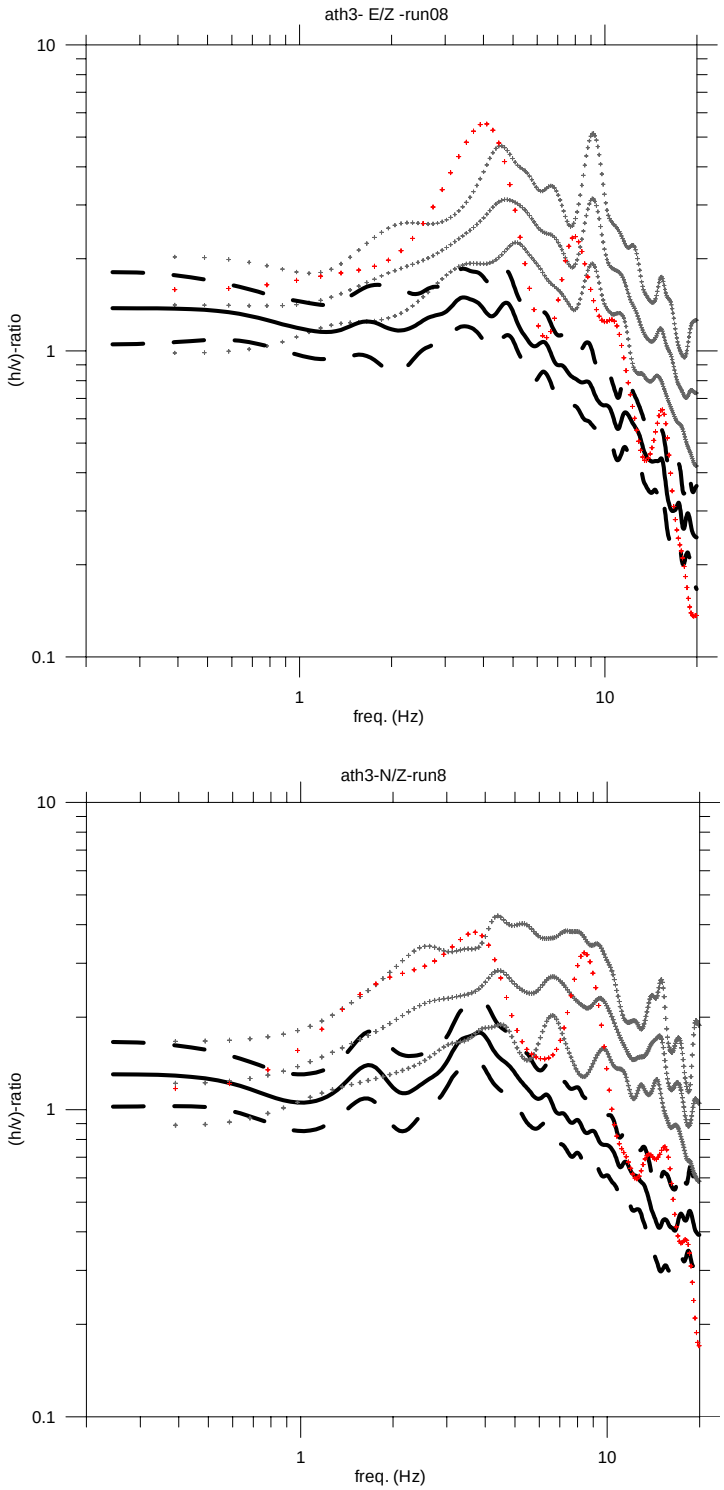

Figure 2. Athens (KEDE) site: strong motion (red), weak motion (gray) and ambient noise (black): E-W/Z (upper graph) and N-S/Z (lower graph).

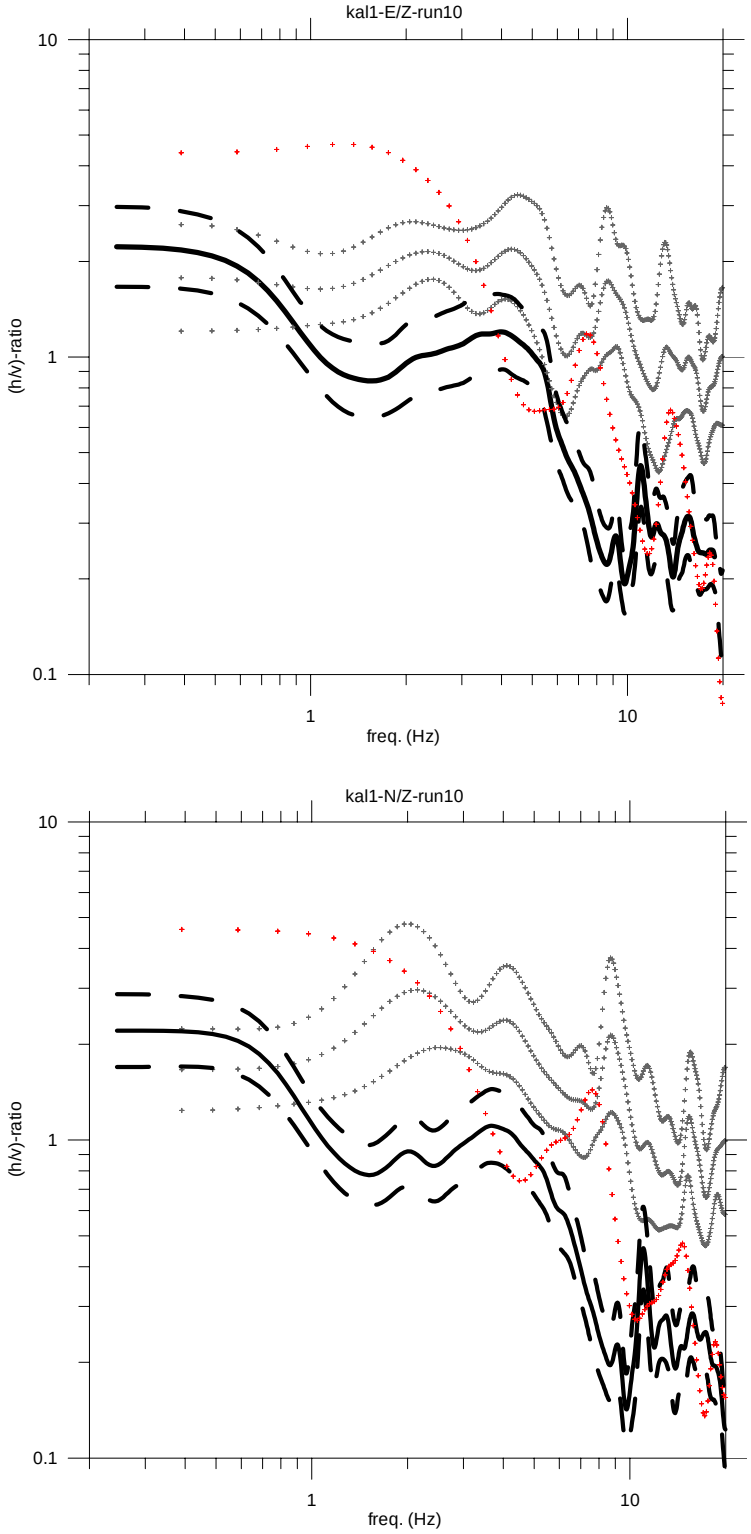

Figure 3. Kalamata site: strong motion (red), weak motion (gray) and ambient noise (black): E-W/Z (upper graph) and N-S/Z (lower graph).

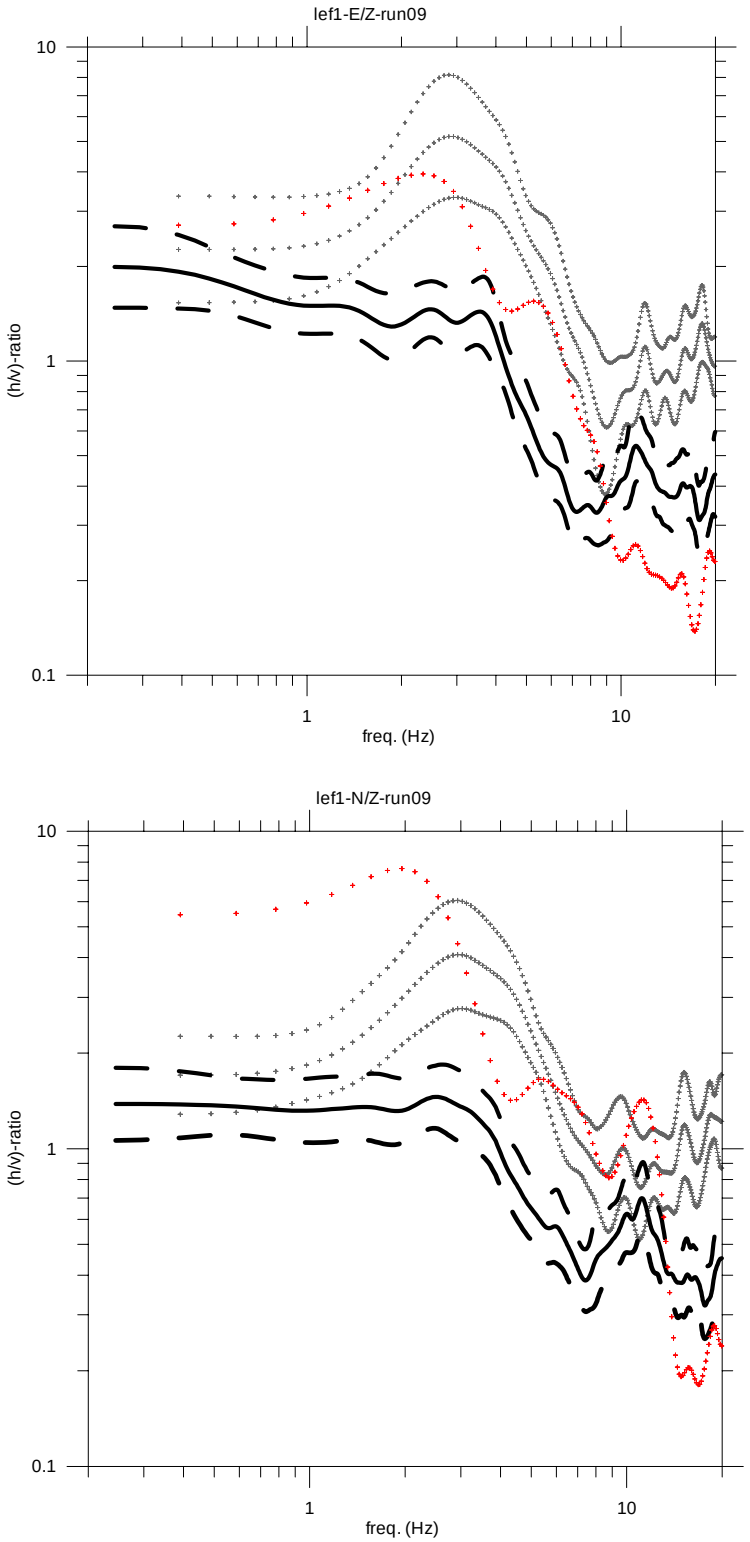

Figure 4. Lefkas site: strong motion (red), weak motion (gray) and ambient noise (black): E-W/Z (upper graph) and N-S/Z (lower graph).

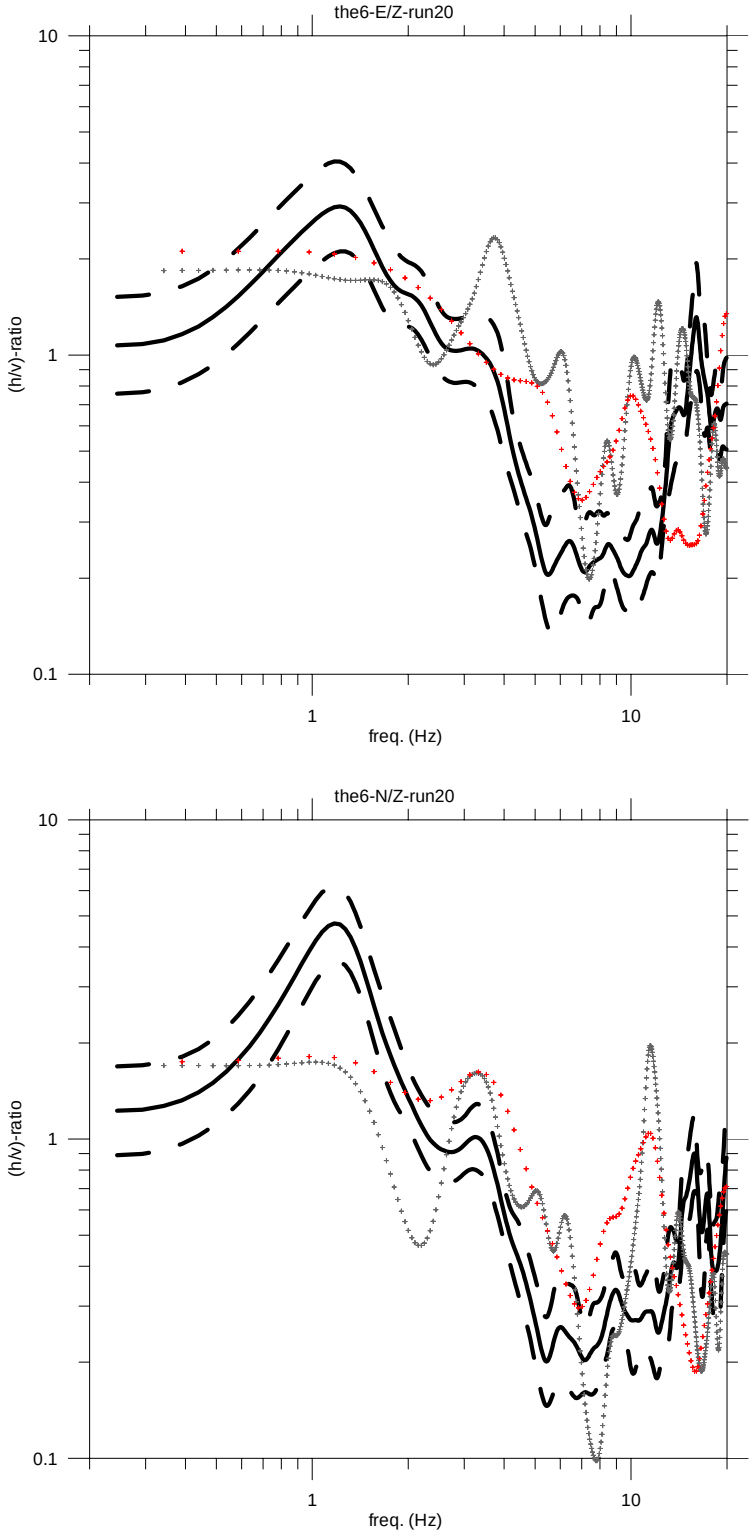

Figure 5. Thessaloniki (City Hotel) site: strong motion (red), weak motion (gray) and ambient noise (black): E-W/Z (upper graph) and N-S/Z (lower graph).

Discussion

Argostoli (Figure 1) is the only example among those considered where there is good agreement between H/V ratios from the three sets of data: strong motion (PGA > 10% g), weak motion and ambient noise. All three display the fundamental site resonance, with the strong-motion ratios being significantly shifted towards lower frequencies, indicative of nonlinear site response. Also notable are the higher values of the strong-motion peaks relative to the other two.

At the Athens (KEDE) site (Figure 2) again there is a notable shift of the resonance frequencies of the strong-motion ratios relative to the weaker ones. The ambient-noise data fail to follow the earthquake data, both in frequency and in amplitude.

In the Kalamata data set (Figure 3) there is some similarity in the shapes of the weak-earthquake and ambient-noise datasets, with the former substantially exceeding the latter in amplitude. The strong-motion ratios are significantly different from the former two datasets, yet exhibiting the characteristic shift in the frequency of the fundamental peak.

At the Lefkas site (Figure 4), the earthquake H/V ratios clearly show the fundamental resonance, with the expected ‘nonlinear’ shift. The ambient-noise curves fail to reveal the fundamental resonance. Interestingly, whereas in the E-W direction the strong and weak earthquake data have a similar resonance-peak amplitude, in the N-S direction the ‘strong’ peak is remarkably higher.

The case of Thessaloniki (City Hotel, Figure 5) stands apart in that it is the only site among those considered where ambient noise reveals a clear fundamental site resonance with earthquake data failing to do so. Noteworthy is the fact that there was only one quality ‘weak’ earthquake recording available at this site.

References

Jarpe, S.P., Cramer, C.H., Tucker, B.E., Shakal, A.F., 1988, A comparison of observations of ground response to weak and strong ground motion at Coalinga, California, *Bull Seism Soc Am* **78**, 421-435.

Darragh, R.B. and Shakal, A.F., 1991, The site response of two rock and soil station pairs to strong and weak ground motion, *Bull Seism Soc Am* **81**, 1885-1899.

Field, E.H., Johnson, P.A., Beresnev, I.A. and Zeng, Y, 1997, Nonlinear ground-motion amplification by sediments during the 1994 Northridge earthquake, *Nature* **390**, 599-602.

Field, E.H., Kramer, S., Elgamal, A.-W., Bray, J.D., Matasovic, N., Johnson, P.A., Cramer, C., Roblee, C., Wald, D.J., Bonilla, L.F., Dimitriu, P.P. and Anderson, J.G., 1998, Nonlinear site response: where we're at, *Seism Res Letters* **69**, 230-234.

Aguirre, J. and Irikura, K., 1997, Nonlinearity, liquefaction, and velocity variation of soft soil layers in Port Island, Kobe, during the Hyogo-ken Nanbu earthquake, *Bull Seism Soc Am* **87,** 1244-1258.

Beresnev, I.A., Field, E.H., Van Den Abeele, K. and Johnson, P.A., 1998, Magnitude of nonlinear sediment response in Los Angeles basin during the 1994 Northridge, California, earthquake, *Bull Seism Soc Am* **88**, 1079-1084.

Beresnev, I.A., Atkinson, G.M., Johnson, P.A. and Field, E.H., 1998, Stochastic finite-fault modeling of ground motions from the 1994 Northridge, California, earthquake. II. Widespread nonlinear response at soil sites, *Bull Seism Soc Am* **88**, 1402-1410.

Hartzell, S., 1998, Variability in nonlinear site response during the 1994 Northridge, California, earthquake, *Bull Seismol Soc Am* **88,** 1426-1437.

Cultrera, G., Boore, D.M., Joyner, W.B., and Dietel, C.M., 1999, Nonlinear soil response following the 1994 Northridge, California, earthquake, *Bull Seism Soc Am* **89**, 1214-1231.

Borcherdt, R.D., 1970, Effects of local geology on ground motion near San Francisco Bay, *Bull Seism Soc Am* **60**, 29-61.

Cranswick, E., 1988, The information content of high-frequency seismograms and the near-surface geologic structure of "hard rock" recording sites, *Pageoph* **128**: 335-363.

Steidl, J.H., Tumarkin, A.G. and Archuleta, R.J., 1996, What is a reference site? *Bull Seism Soc Am* **86**, 1733-1748.

Boore, D.M. and Joyner, W.B., 1997, Site amplification for generic rock sites, *Bull Seism Soc Am* **87**, 327-341.

Dimitriu, P., Kalogeras, I. and Theodulidis, N., 1999, Evidence of nonlinear site response in HVSR from near-field earthquakes, *Soil Dyn Earthquake Engng* **18**, 423-436.

Dimitriu, P., Theodulidis, N. and Bard, P.-Y., 2000, Evidence of nonlinear site response in SMART1 (Taiwan) data, *Soil Dyn Earthquake Engng* **20**, 155-165.

Dimitriu, P., Theodulidis, N., Hatzidimitriou, P., Anastasiadis, A., 2001, Sediment nonlinearity and attenuation of seismic waves: a study of accelerograms from Lefkas, western Greece, *Soil Dyn Earthquake Engng* **21**, 63-73.

Dimitriu, P., 2002, The HVSR technique reveals pervasive nonlinear sediment response during the 1994 Northridge earthquake (Mw 6.7), *J of Seismology* **6**, 247-255.